Luminosity Monitoring for PrimEx

Contributing authors: ....

June 23, 2003

Contents

1 Abstract **4**
1.1 PrimEx error budget 4

2 Basic philosophy of tagged photon flux determination **4**
2.1 The Tagged Photon System 4
2.2 Absolute calibration with total absorption counter 5
2.3 Relative calibration with pair spectrometer 6

3 Summary of tagger improvements (E. Pasyuk) **6**

4 Total absorption counter (Mahbub) **7**
4.1 Placement of TAC on beamline (Dale) 7

5 Pair Spectrometer **9**
5.1 Description of device (D. Dale) 9
5.2 Status of data analysis (Aram, D. Dale, I. Nakagawa) 9
5.2.1 Analysis tasks to do 14

6 Electron counting by sampling method(Dave L.) **14**
6.1 Introduction 14
6.2 DeadTimes 16
6.2.1 DAQ 16
6.2.2 Multihit TDC 16
6.3 Total Photon Flux for Experimental Cross Section 17
6.3.1 Trigger Condition 17
6.3.2 Tagged Photo-π^0 Cross Section 17
6.3.3 Additional Thoughts With Respect to Electron Scattering Experiment 19
6.3.4 What's wrong with the Conventional Scalor Ratio Deadtime Correction? 19
6.4 Methods of Calculating Detector Rates 19
6.4.1 The Exponential Method 19
6.4.2 The Integral Method 22
6.4.3 The Poisson Method 22
6.5 Errors 24
6.5.1 Systematic Errors Due to Beam Instability 24
6.5.2 Statitical Errors 25
6.6 Summary 25
6.6.1 JLab beam current stability 25

7 Trigger selection for luminosity monitoring events (D. Sober, E. Pasyuk, D. Dale, D. Lawrence) **25**
7.1 Pair spectrometer rates with a MOR trigger 26

8 Target thickness measurements (R. Miskimen) **26**

9 Normalizing Primakoff yield to Compton yield (D. Dale) **28**
9.1 The basic idea . . . 28
9.2 Identification of the Primakoff events . . . 28
9.3 Sensitivity of method to energy calibration . . . 34
9.4 Sensitivity to HYCAL central hole size . . . 34
9.5 Conclusion . . . 34

10 Beamline instrumentation **40**
10.1 Electron beam position monitors . . . 40
10.2 Harp . . . 40
10.3 Online scintillating fiber based profile monitor (Liping) . . . 40

11 Future test run plans **40**

12 Appendix I: Current Luminosity Monitoring Runplan **41**

13 Appendix II: Technical Details of Pair Spectrometer **41**
13.0.1 Detectors . . . 41

1 Abstract

Determination of the luminosity (tagged photon flux and target thickness) for the PrimEx π^o lifetime experiment represents the largest contribution to the experimental uncertainty of the measurement. This document is meant to summarize our approach to this issue. It is meant to be a living document which will be updated from time to time, as we progress.

1.1 PrimEx error budget

We intend to control the experimental errors to make a measurement of the π^o lifetime with a less than 1.5% precision. The various contributions to this error are shown below, where it can be seen that the target thickness and photon flux are the dominant errors:

statistical	0.4%
target thickness (atoms/cm^2)	0.7%
photon flux	1.0%
π^o detector acceptance and misalignment	0.4%
background subtraction	0.2%
beam energy	0.2%
distorted form factor calculation errors	0.4%
total	1.4%

2 Basic philosophy of tagged photon flux determination

2.1 The Tagged Photon System

The primary advantages of the *PrimEx* experiment over the previous Primakoff experiments arise from the possibility of using the Jefferson Lab Hall B tagging facility to carefully control systematic errors and reduce backgrounds. First, the tagging technique will enable a significantly more accurate knowledge of the photon flux. Second, due to the energy dependence of the Primakoff cross section, it is critical to have a good knowledge of the absolute photon beam energy.

We will use a 6 GeV electron beam incident on a thin (10^{-4} radiation length) bremsstrahlung converter foil. The post-bremsstrahlung electrons will be momentum analyzed in the Hall B photon tagger magnet and photons will be tagged in the energy range from 4.6 to 5.7 GeV. The Hall B bremsstrahlung photon tagging system spans the photon energy range of 20% to 95% of the incident electron energy. The detector system consists of two planes of counters: 384 overlapping scintillators which define 767 fine energy channels of width 0.001

E_e (the "E" counters), and 61 larger scintillators, each read out by two photomultiplier tubes and designed for good time resolution (the "T" counters). The sizes of the T-counters are designed to produce approximately equal counting rates in two groups. When all 61 T-counters are used, the total tagging rate can be as high as 50 MHz for the whole focal plane. Counters T1-T19, which span the photon energy range from 77% to 95% of E_e, are proportionally smaller than the others, and will allow a tagging rate of up to 50 MHz in this region alone. This experiment will use only the "high-rate" counters T1-T19. The tagger trigger signal will be formed by taking the coincidence of the left and right PMT's of the T-counters, while the tagger Master OR (MOR) will be produced by ORing the T-counter coincidence channels.

2.2 Absolute calibration with total absorption counter

Since each π^o decay event is measured in coincidence with a tagging counter signal, the normalization of the cross section to the incident photon flux depends on knowing the number of tagged photons on target in each energy bin during the run. The number of tagged photons on target is not necessarily equal to the number of events recorded by the tagging counters because of a number of effects:

(1) events in which a bremsstrahlung photon is produced but is absorbed before reaching the target.

(2) Møller scattering events in the bremsstrahlung radiator which produce an electron in the tagging counters without an accompanying photon.

(3) Extra post bremsstrahlung electrons registered due to room background.

Events of the first type will be minimized by allowing the entire bremsstrahlung beam to travel in vacuum without collimation to the target. The second category of events is known to affect the tagging rate at the level of a few percent. The combination of these first two effects can be measured by performing a calibration run in which the Primakoff target is removed and a lead glass total absorption counter (TAC) is placed in the photon beam. The ratio of Tagger·TAC coincidences to tagger events, the so called tagging ratio, is then recorded.

Knowing this ratio, one can determine the photon flux in the data taking run by counting the number of post bremsstrahlung electrons in a given tagging counter:

$$N_\gamma^{tagged}(experiment) = N_e(experiment) \times \frac{N_\gamma^{tagged}(calibration)}{N_e(calibration)} \tag{1}$$

One can then determine the cross section from the tagged yield of π^o's:

$$\text{TaggedYield} = \frac{d\sigma}{d\Omega} \times t \times \Delta\Omega \times N_e(experiment) \times \frac{N_\gamma^{tagged}(calibration)}{N_e(calibration)}, \tag{2}$$

where t is the target thickness, and $\Delta\Omega$ is the solid angle of the pion detector. In the calibration run, the total absorption counter rate is limited, and, therefore, the tagging efficiency must be measured at a rate which is reduced by a factor of about one hundred as compared to the data taking run. As such, any rate dependence in the tagging efficiency must be considered. Note that in equation 2.2, both the tagged yield (coincidence of π^o and tagging electron) and $N_e(experiment)$ (number of tagging electrons) are both affected by the deadtime associated with the tagging counters in a similar fashion.

2.3 Relative calibration with pair spectrometer

The use of the total absorption counter to calibrate the number of photons per tagging electron will provide an absolute calibration of the photon flux incident on the π^o production target. However, these measurements will be performed at intervals throughout the data taking, and will by necessity be performed at an electron beam current which is two orders of magnitude less than the production data taking runs. Consequently, we have constructed a pair production luminosity monitor which will measure the relative tagged photon flux over a range of intensities, and will operate continuously throughout the data taking runs.

The pair spectrometer will use the physics target as a converter, and will make use of the 15 kgauss-meter dipole magnet placed just downstream of it. The electrons and positrons are detected on either side of the beam in a series of plastic scintillator telescopes. The requirements of the pair spectrometer are that it must operate over the entire range of intensities (of both the flux calibration and data taking runs) and have a smooth, relatively flat acceptance in E_γ covering the entire tagging range. The segmentation of the pair spectrometer detectors is driven by the fact that the pair production and Primakoff target are the same, and therefore the pair spectrometer detectors must accommodate the rates from a 5% radiation length target. Under the PrimEx run conditions, we expect singles rates on a single telescope to be about 140kHz, and a total of 90kHz of pair spectrometer-tagger coincidences over the range of tagging energies from $0.77E_o$ to $0.95E_o$. The efficiency of the pair spectrometer for tagging photons will be about 0.6%. A schematic of the pair spectrometer with one simulated pair production event is shown in figure 1. Each arm presently consists of eight telescopes with overlapping momentum acceptances placed symmetrically on either side of the beamline. We are currently in the process of upgrading this to 16 telescopes on each side (for a total of 64 detectors) to provide the ability to tag photons over nearly the entire range of the Hall B tagger, from $0.2E_o$ to $0.95E_o$.

3 Summary of tagger improvements (E. Pasyuk)

Upgrades to the tagger E counters have been performed, and they are largely in good shape. New E counter electronics are currently being fabricated and tested in Italy. These electronics are expected to greatly improve instability problems in the E counters, as well as providing greatly improved flexibility in that thresholds, delays, and gate widths will be fully programmable. This software is being developed by the Glasgow group. Two pieces of hardware that are still needed are (1) VME crates and (2) a module to make the MOR.

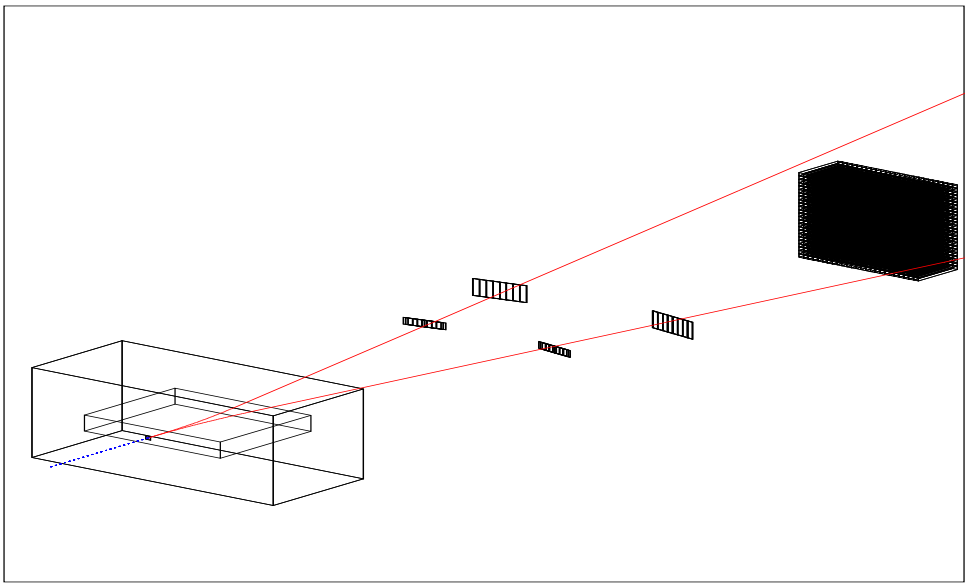

Figure 1: Layout of the luminosity monitor and one pair production event. Each detector arm is currently segmented into eight contiguous plastic scintillator telescopes.

4 Total absorption counter (Mahbub)

The total absorption counter (TAC) consists of a single $20 \times 20 \times 20 \times 40 cm^3$ lead glass block (SF5, $L = 17X_o$). It has a single 5" Hamamatsu PMT (R1250, rise time $\sim 2.5ns$) attached to it and is instrumented with both an ADC and TDC. It will be mounted on a support structure with vertical motion.

In the August 2002 test run, with a 100 pA electron beam and a $2\times10^{-5}X_o$ bremsstrahlung radiator, the TAC fired at about 100kHz with a 35 mV threshold.

The absolute normalization of the experiment hinges upon the assumption that the TAC has 100% efficiency for detecting photons in the tagging energy range. As such, studies of the tagging ratios as a function of TAC threshold are necessary.

In August 2002, the TAC was commissioned. Figure 2 shows the measured tagging ratios across the tagged photon energy range from 0.77 to $0.95\%E_o$. (As a technical point, the TDC self inhibit time had to be taken into account.) Given that there was a $5\%X_o$ target in place, the tagging ratios are close to what one would expect. Further studies without a target and with varying tagging rates are needed.

4.1 Placement of TAC on beamline (Dale)

Geant simulations to determine if it can be placed behind HYCAL

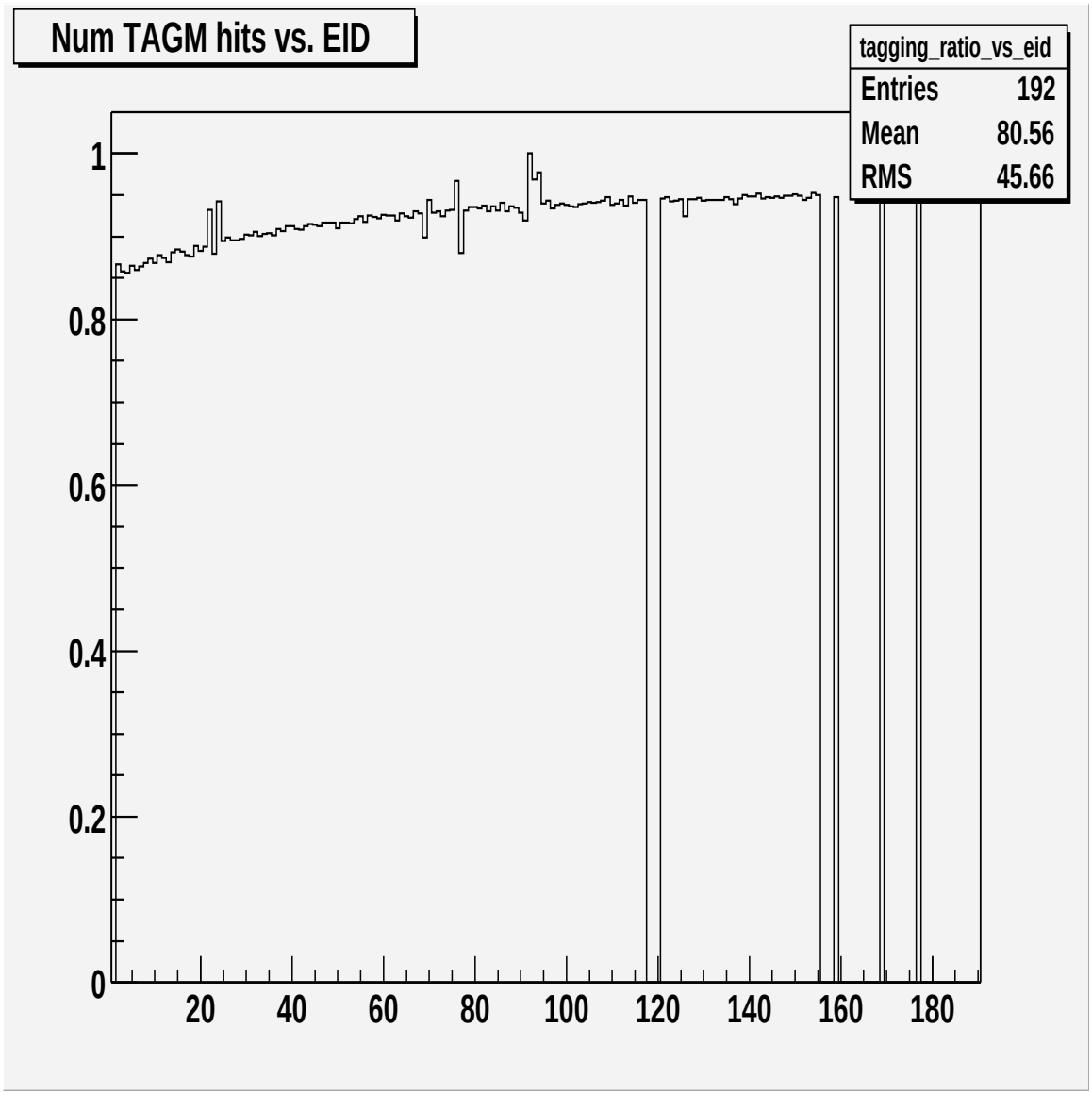

Figure 2: Tagging ratio as measured with the PrimEx TAC in August 2002 test run. A $5\% X_o$ target is placed at the PrimEx target postion between the bremsstrahlung radiator and the TAC.

5 Pair Spectrometer

5.1 Description of device (D. Dale)

5.2 Status of data analysis (Aram, D. Dale, I. Nakagawa)

In August 2002, we performed a series of beam tests to ascertain whether the relative tagging efficiencies, as measured by the pair spectrometer, were independent of the beam current at the one percent level. This involves beam currents ranging from those in which the PrimEx data taking will occur on the high end, to those in which the calibration with the TAC will be performed on the low current end. For TAC calibration runs, we measure the absolute tagging ratio:

$$R_{absoulute} = \frac{N^{TAC}_{\gamma \cdot e_i}}{N_{e_i}} \tag{3}$$

where $N^{TAC \cdot e_i}_{\gamma}$ is the number of photons, as measured in the TAC, in coincidence with tagging counter i, and N_{e_i} is the number of electrons in tagging counter i. With the pair spectrometer, we can measure the relative tagging ratio:

$$R_{relative} = \frac{N^{ps}_{e^+e^- \cdot e_i}}{N_{e_i}} \tag{4}$$

where $\frac{N^{ps}_{e^+e^- \cdot e_i}}{N_{e_i}}$ is the number of pair production events in coincidence with a given tagging counter. While this is a relative number, its normalization can be fixed with the TAC, and it has the advantage of the possibility of measurement over all relevant currents, *i.e.* the high currents of the production data taking and the low currents at which the absolute tagging ratios are measured with the TAC. In August 2002, we measured $R_{relative}$ from 0.08 to 100 nAmps, and the results are shown for one T counter (T5) in figure 3. As can be seen, $R_{relative}$ is quite independent of the beam current. In these, and all subsequent plots, only the T counters were taken into consideration (no E-T coincidences), and accidentals between the pair spectrometer and the tagger were subtracted.

Figures 4 and 5 show the relative tagging ratios across the tagger focal plane. The energy dependence of $R_{relative}$ arises from that of the pair production cross section as well as the energy acceptance of the pair spectrometer as determined by the acceptances of the pair spectrometer detectors and the pair spectrometer magnetic field setting.

A GEANT simulation of the efficiency of the pair spectrometer to tag a photon of a given energy (under the conditions of the August 2002 run) is shown in figure 6. If the absolute tagging efficiency is flat in energy, one would expect the shapes of the curves in figures 4, 5 and 6 to be roughly the same. The fact that they are not can be attributed to (1) the energy dependence of the pair production cross section, or more likely, (2) deficiencies in the magnetic field representation in the GEANT simulation. Since the B field in the simulation is a simple, uniform field, in all probability the $B \cdot dl$ was in reality higher than that in the simulation. While such issues are being investigated, the magnitude of the efficiency of the pair spectrometer to tag a photon is roughly as expected ($\sim 0.5\%$).

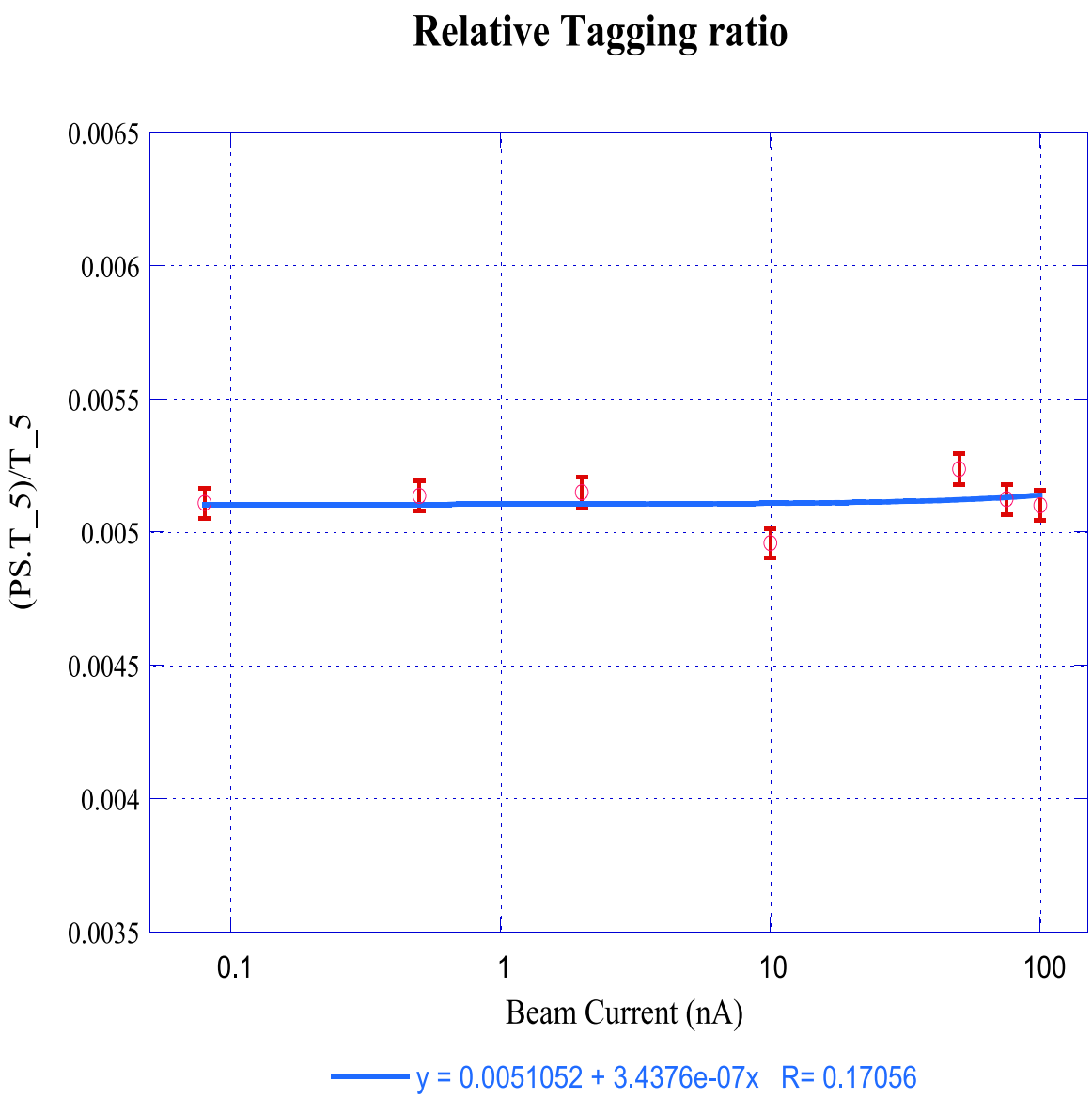

Figure 3: Measured relative tagging ratios for T counter 5 as a function of nominal electron beam current.

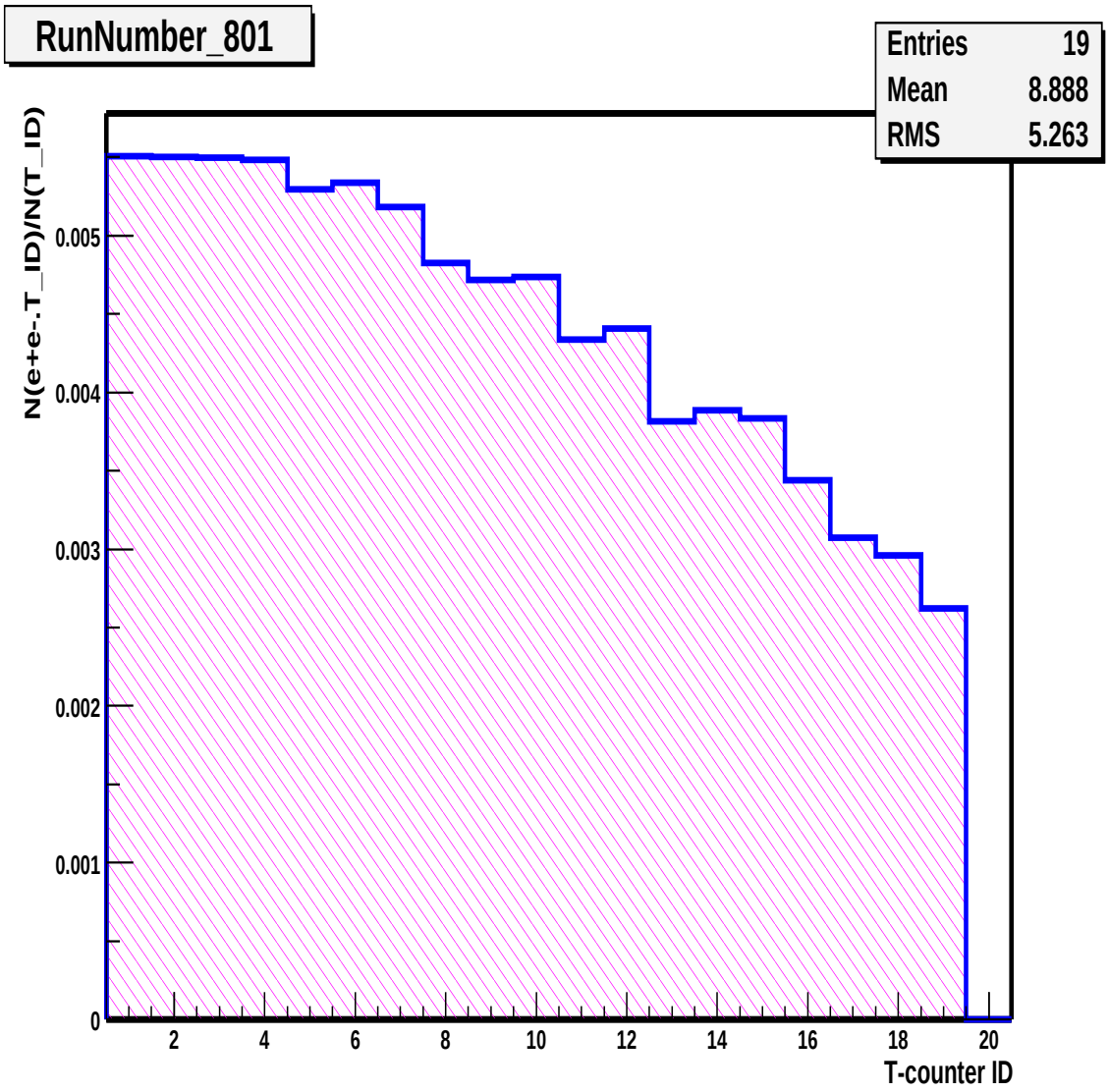

Figure 4: Relative tagging ratios for each of the 19 T counters for run 801.

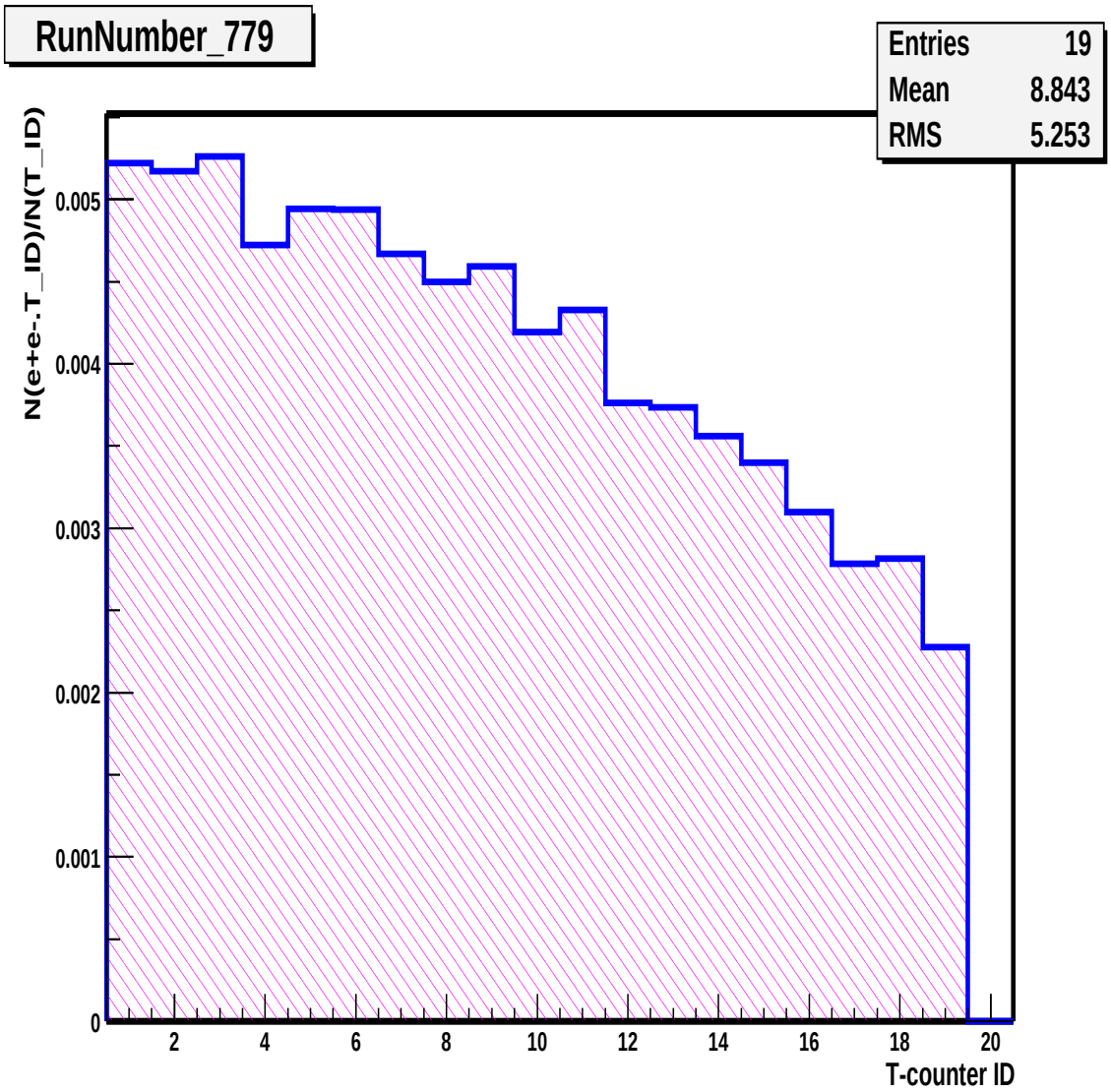

Figure 5: Relative tagging ratios for each of the 19 T counters for run 779.

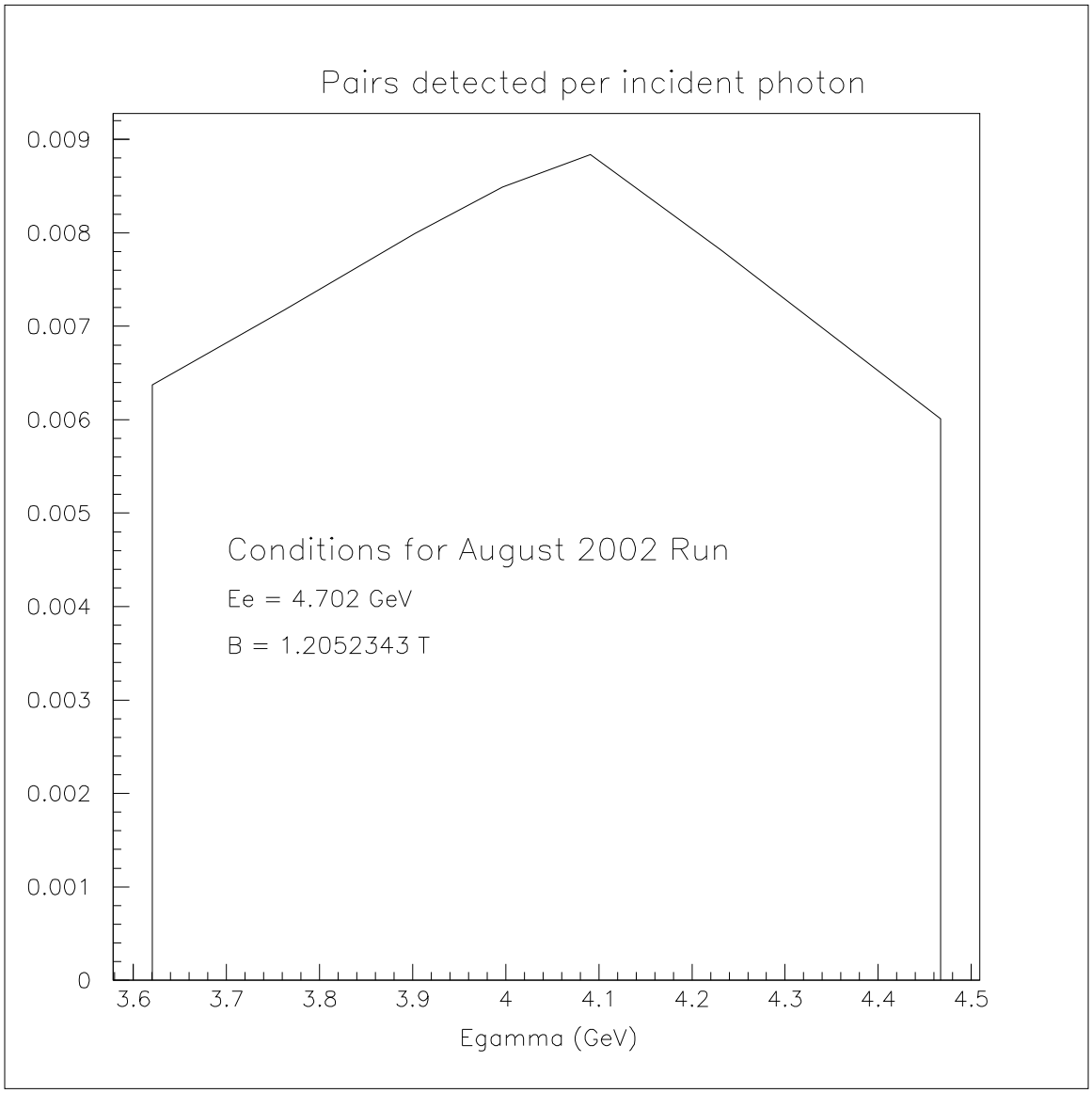

Figure 6: Calculated efficiency for the pair spectrometer to tag a photon of a given energy under the conditions of the August 2002 run.

To combine information from all 20 T counters, we (as in Aram) have proceded as follows. For a given T counter, we have calculated the average relative tagging efficiency, where the average is over the seven different currents of the run. Then, for each beam current and each T counter, we have calculated the deviation from the average for each T counter. This gives:

$$\frac{\delta R_{relative}}{R_{relative}} = 5\% \tag{5}$$

Improvements to this should be forthcoming. This 5% error does not take into account statistical errors. Specifically, the statistical error due to accidentals subtraction at high currents has not been taken out of the 5% dispersion. This needs to be worked on.

It is worth noting that the above analysis was done using a MOR trigger. That is, the $PS \cdot T_i$ coincidences were determined from the associated TDC spectra, and the number of electrons for a given tagging counter were determined by the coincidence in the TDC spectrum of T_i with the MOR.

5.2.1 Analysis tasks to do

- Implement E-T coincidences, but still bin by T counters..
- Deconvolute statistical fluctuations due to accidentals subtraction from distribution of deviations of relative tagging efficiencies from the mean.
- Utilize energy information from pair spectrometer to minimize accidentals, *i.e* implement $E_{e^+} + E_{e^-} > E_\gamma$ cut.
- Remove periods associated with beam trips from the analysis.

6 Electron counting by sampling method(Dave L.)

6.1 Introduction

An important component in calculating the photon flux is counting the number of electrons detected by the tagger or, more precisely, have the *potential* of being detected. One traditional method of counting detector hits is using scalers which is discussed in section 6.3.4. Another method is based on TDC information which can be used to require strict coincidences between detectors in software. A multi-hit TDC is capable of recording lots of information for a limited window in time. In practical applications, the average time between events is much larger than this window. This leads to a situation where the recorded data are simply samples of what the detectors saw throughout the course of a run. The assumption is then made that these samples are representative of detectors' responses for the times when no data is recorded. The recorded data can then be used to calculate detector rates which are integrated over the live time of the experiment (see section 6.2).

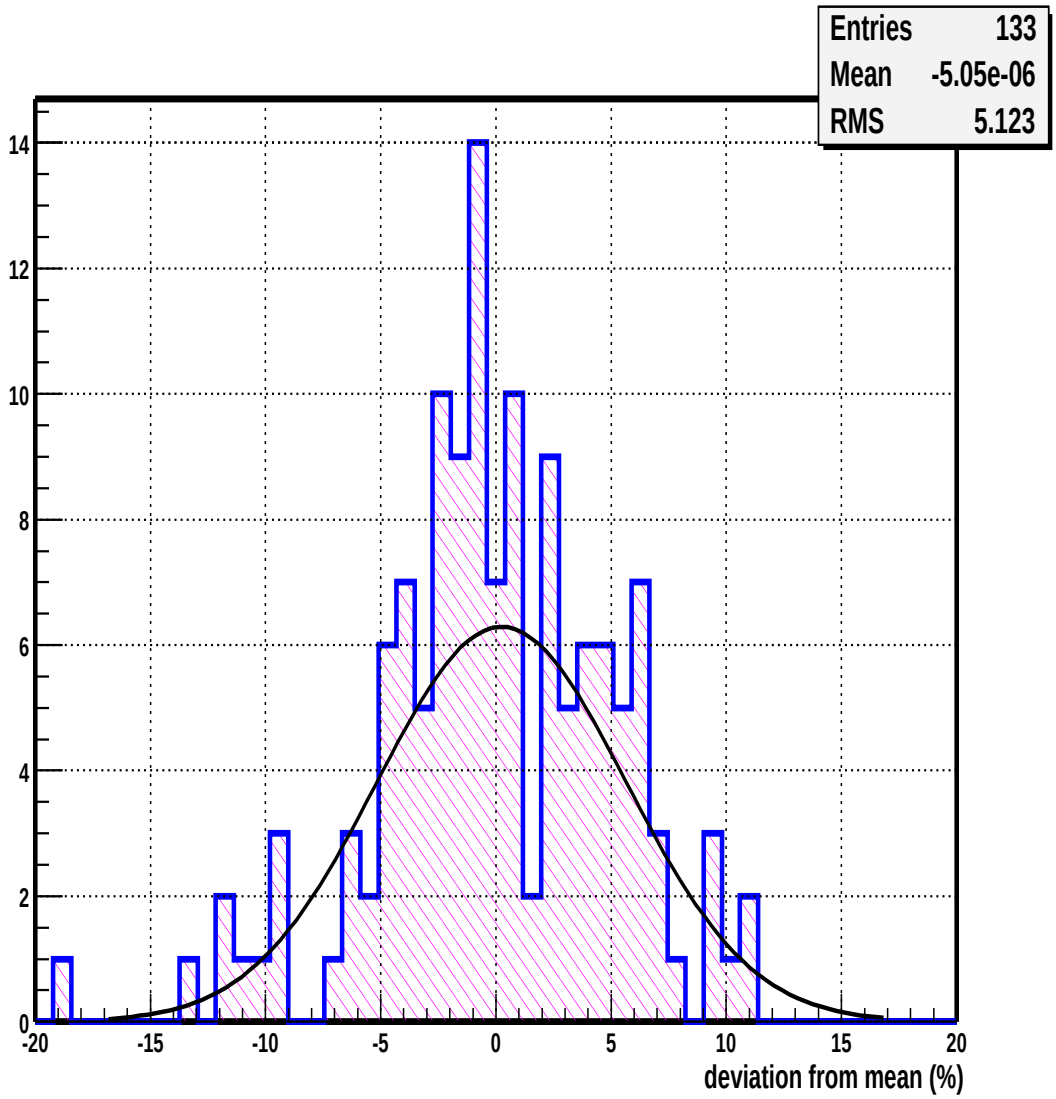

Figure 7: The difference in relative tagging ratio for each T counter from the mean for each of the seven different runs done at different beam currents (19 T counters $\times$ 7 runs = 133 entries.

6.2 DeadTimes

There are three different types of an intrinsic deadtime in the PrimEx hardwares associate with measuring π^0 production. One is in the DAQ system and other two are associated with the multihit TDC module LRS1877. Note that not every deadtime presented here necessarily needs to be corrected for in order to obtain the π^0 photoproducion cross section. The detailed reasons for this will be described in section **??**.

6.2.1 DAQ

LiveTime of DAQ: This is the intrinsic deadtime of the data acquisition system. This deadtime is measured by taking the ratio of two scalers, which are dedicated to measuring the livetime[1] Both scalers are driven by a 200 kHz internal clock. One is livetime gated while the other is free running.

6.2.2 Multihit TDC

25 ns Self Inhibit DeadTime The LRS1877 has roughly about a 25 ns double pulse resolution. This means any subsequent hit which comes within 25 ns after a previous hit won't be recorded. Consequently the 25 ns after any incoming signal should be treated as a intrinsic deadtime of that particular TDC channel.
LIFO: The LRS1877 TDC module has a programmable LIFO(Last In First Out) up to 16 hits per event per channel. As shown in Figure 8, it records incoming hits into LIFO memory cumulatively. When it receives a common stop signal, it takes a "snapshot" of these multiple hits recorded within the past Δt nanoseconds and dumps them into the data stream.

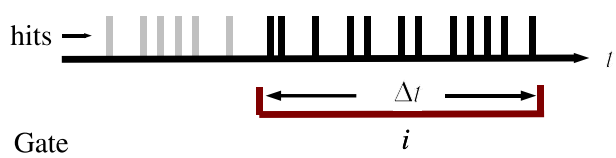

Figure 8: Multihit recording per event (gate). The LRS1877 can hold multiple hits (black ticks) in a single event (gate). All hits (black ticks) in the TDC gate i are recorded into the data stream.

However, if a channel gets more hits in a single event than the LIFO can hold, the oldest hits are replaced with the newest ones. As shown in Fig.8, grayed out events are cleared and not be recorded in the data even though these hits are happening within the TDC time window Δt.

[1] The effective time window for the data aquisition to be ready or active.

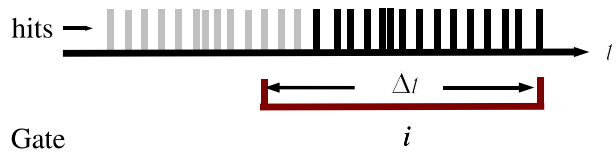

Figure 9: The LIFO (Last In Fast Out) memory feature of LRS1877. If hits are more than the maximum hits LRS1877 can hold, then the oldest hits (gray ticks) are cleared from the memory and replaced by newest ones.

6.3 Total Photon Flux for Experimental Cross Section

In section **??**, hardware deadtimes affecting PrimEx were discussed. So what kind of corrections do we need to apply to the photon hits accumulated in the TDC module in order to obtain the total number of photons for the cross section calculation? The quick answer to the question is that the corrections associated with the TDC deadtimes described in the previous section are not neccessary[2] This is deeply associated with the PrimEx triggering conditions. Let's start by looking at the triggering conditions first and then move on to a discussion of the cross section formula and why we don't need the corrections.

6.3.1 Trigger Condition

The primary trigger for the PrimEx experiment is formed by HYCAL. Once a multiple cluster event is observed in HYCAL, then a trigger is formed. Once the trigger is formed, the LRS1877 multihit TDC send a "snapshot" of tagger hits with respect to the timing signal from HYCAL. Presented in Figure. 10 is a schematic diagram of the trigger and DAQ for a typical π^0 event. Note it is important to keep this in your mind for later argument that the tagger is **not** used to form the trigger for π^0 events in this experiment. The π^0 event trigger is formed by HYCAL. This is because of the data aquisition will be swamped by the extremely high rate of tagger signals, most of which represent photons that just go through the target without producing a π^0. It is much more efficient to form the primary trigger by π^0 event in the HYCAL.

6.3.2 Tagged Photo-π^0 Cross Section

The experimental π^0 photoproduction cross section is given by following fomula:

$$\frac{d\sigma}{d\Omega} = \frac{Y_{\pi^0}}{N_{\gamma}^{\text{hits total}} d\Omega} \tag{6}$$

where

Y_{π^0} : Total number of π^0 induced by TAGGED photons in livetime

[2]Then why do we care about the TDC deadtime? Actually the knowledge of these deadtime are necessary for consistency check among different approach to estimate detector/tagger rates. See Section 6.4 for details.

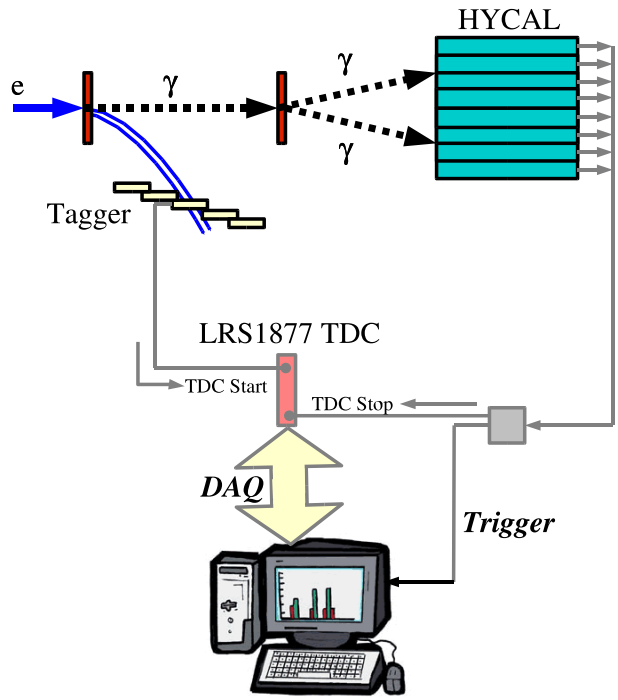

Figure 10: A schematic diagram of trigger and DAQ for typical π^0 event. The multihit TDC records cumulative hits until a common TDC stop signal is arrived from HYCAL.

$$N_\gamma^{\text{hits total}} \quad : \quad \text{Total number of TAGGED photons in livetime}$$
$$d\Omega \quad : \quad \text{solid angle of photon}$$

Here one has to carefully define Y_{π^0} and $N_\gamma^{\text{hits total}}$. As it is defined above, Y_{π^0} is supposed to be the total number of π^0 events induced by TAGGED photons, **NOT** total π^0 events observed by the HYCAL. As is the fact the primary trigger is not induced by the tagged photons, but by the HYCAL, there are possible π^0 events in the data which are induced by not TAGGED photons. These π^0 events which are missed to be observed partner electrons in the tagger have essentially no capability to reconstract a missing mass. Thus these events supposed to be excluded from a consideration. We account only π^0 events which are TAGGED as true events.

In order to keep the consistency of the numerator and the denominator in the Eq.6, $N_\gamma^{\text{hits total}}$ has to be counted consistently with the way Y_{π^0} is estimated. In this way we would rather concern about number of **tagged** photons, which may potentially be less than number of actuall photons sent into the physics target. The event which missed electrons in the tagger TDC due to the deadtime won't have a potential to reconstruct the missing mass even if π^0 is induced by these photons. Thus these missing tagged electron (photon) events due to the TDC deadtime should be excluded from the total photon flux estimation in the denominator of the cross section formula Eq.6. Thus the discussion is focused on rate estimate for tagged photons. Various approachs to estimate the rate are described in the

following section.

6.3.3 Additional Thoughts With Respect to Electron Scattering Experiment

For those of whose knowledge about the deadtime correction is heavily biased by the electrons scattering experiment, it is important to aware of that the deadtime correction for the tagged photon experiment is done in totally different senario. In electron scattering experiment, the number of electrons bombered a target is measured through beam current. A typical correction raise from computer deadtime of detector electronics, but not for the beam charge, because the beam charge is usually measured in computer deadtime free method. Thus the experimental cross section is given by a total number of physics events accumulated in the data corrected by computer deadtime devided by total number of electrons bombered through the target. Here the number of electons bombered though the target is equivalent with total beam charge acquired in the data. On the other hand, the PrimEx cross section won't be given by the total photon flux at the target, but total tagged photon flux at the target. This way the deadtime for π^0 yeild in numerator and total tagged photon flux in demoninator are correlated somewhat each other, therefore correction will be canceled for cross section calculation. Thus a recoverly of π^0 yeild due to the deadtime by applying correction factor is not necessary.

6.3.4 What's wrong with the Conventional Scalor Ratio Deadtime Correction?

It is a standard and well-established techique to use two scalers to calculate a dead time effect of a paticular electronics module. The computer dead time correction factor is given by taking the ratio of a computer inhibited scaler and not inhibited one. The dead time correction for many of electronics modules work out in this manner and in fact the livetime of the DAQ for this experiment will be measured using scalers. However, this does not necessarily work for the deadtime correction of the multihit TDC (LRS1877), because of its LIFO (Last In First Out memory) feature.

6.4 Methods of Calculating Detector Rates

There exist several possible methods for calculating detector rates based on multi-hit TDC data. This section describes 3 such methods. They all, more or less, rely on the fact that events are uncorrelated with one another. This leads to some well known distributions arising purely from statistics. Each has its own benefits and drawbacks which are discussed in the respective sections. Ultimately, all may be used to provide a consistency check.

6.4.1 The Exponential Method

The exponential method uses the time differences between hits to determine the rate at which a detector is firing. For a detector firing at a constant rate, the probability per unit time of a detector firing is constant. This leads to an exponential distribution of the time differences. This is completely analogous to nuclear decay. This is also a very clean way of

determining the true rate of a detector. This provides several distinct benefits over other methods, but has its drawbacks as well. These will be outlined below.

There is a correction that must be applied when histogramming the time differences. This arises due to the finite time window over which the TDC samples for every event. With a 10 μs time window, the only way to obtain an event with a 10 μs time difference is if the first hit is at the very beginning of the window. If it occurs any later, then the second hit will be missed since it will occur outside of the time window. By contrast, one can get 100 ns time differences if the first hit happens anywhere in the first 9.9 μs of the window. A statistical correction must therefore, be applied. The correction is made by weighting each entry in the histogram by the factor:

$$\frac{\Delta t}{\Delta t - T_{diff}} \tag{7}$$

Where T is the TDC window width and tdiff is the time difference between hits. Note that this is NOT a rate dependent correction. The values of T and tdiff are known to the resolution of the TDC (0.5 ns for the LRS1877 that will be used in PrimEx).

Figure 11 shows data from the tagger during the PrimEx test run in summer 2002.

Benefits of the exponential method

- **Not susceptible to LIFO limits** Hits missed due to the TDC LIFO limit only affect the overall normalization of the time difference histogram, not the slope.
- **Independent of TDC multi-hit deadtime** The LRS1877 has a deadtime after each hit of about 25ns. (The effective deadtime is increased for detectors with a discriminator width set larger than this.) The fit to the exponential function can be limited to time differences greater than the deadtime (say, 50ns) where the slope would be unaffected.
- **Function shape is well defined** Any deviation from a purely exponential distribution would indicate problems which have not been accounted for. For example the beam current changing. at some point.
- **All hits are used** Since all hits are uncorrelated, the time difference is not biased by the trigger causing events. Additionally, for detectors which routinely miss hits due to LIFO limits, there is no need to impose a cut before the drop off at early times due to the LIFO. This allows more frequent calculation of the rate which reduces systematic. errors due to beam current drifts.
- **Works for abstract detectors** Since this method is insensitive to deadtime and LIFO effects, detector combinations constructed via software coincidences (which have more complicated LIFO and deadtime dependencies) will also be insensitive.

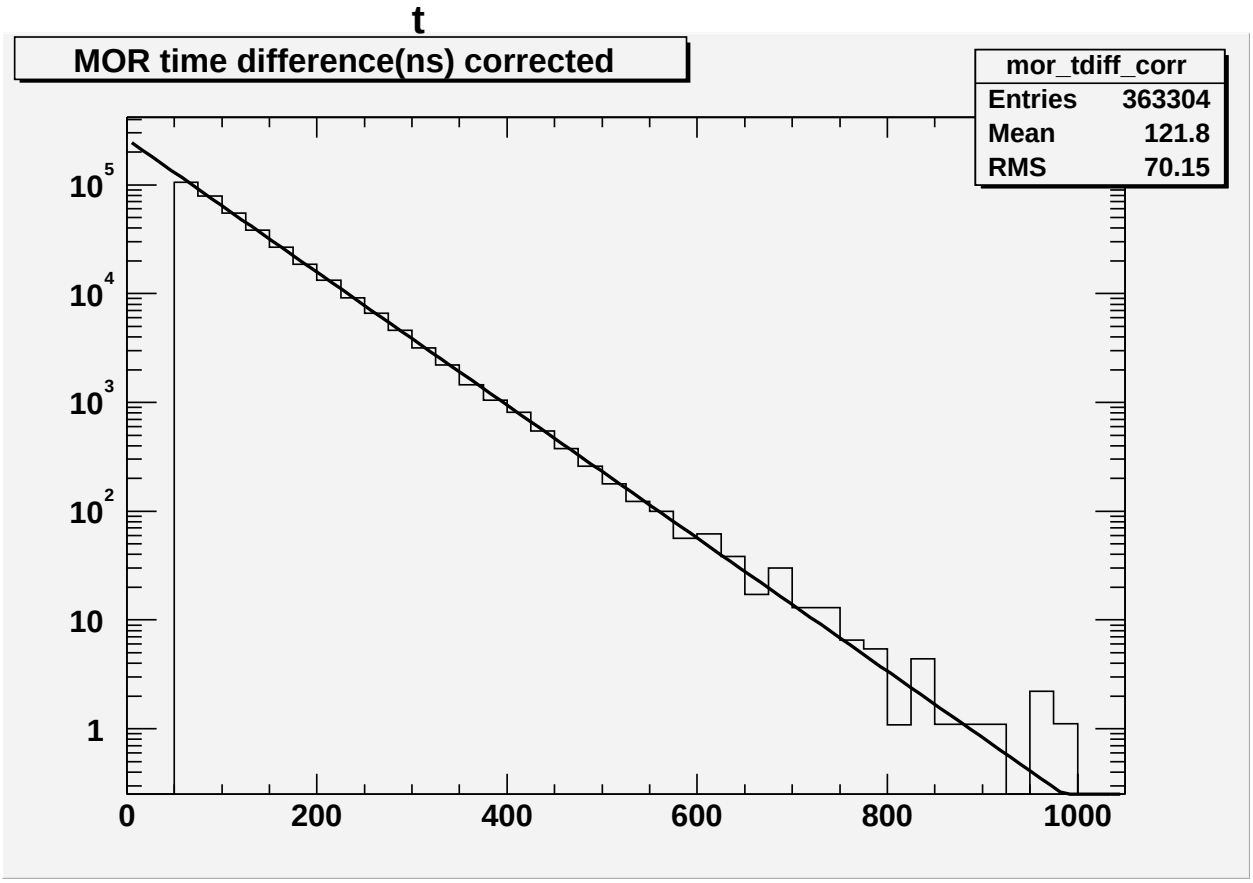

Figure 11: MOR (hardware OR of top 19 Tagger T-counters) time difference distribution after being corrected for the finite time window as described in section 6.4.1. The x-axis is in ns. This is real data from a 75nA PrimEx beam test in 2002. The line is the result of an exponential fit. This figure demonstrates how cleanly the data follows the exponential shape, even over 5 orders of magnitude.

Drawbacks of the exponential method

- **Independent of TDC multi-hit deadtime** The final pi0 yield for the experiment will have missed hits due to the TDC deadtime. The exponential method would measure the rate of electrons in the tagger rather than the rate of detected electrons in the tagger. A correction would have to be applied to account for TDC deadtime.

- **Does not work for low rates** For rates on the order of 1/T and lower (where T is the TDC window width), the slope of the exponential curve becomes very shallow and the relative error becomes very large. The statistics also become quite small because there is an average of 1 hit or less per event.

6.4.2 The Integral Method

The integral method is very straight forward. The time distribution is integrated over a range which excludes the triggering events and any depletion due to LIFO limits. Figure 12 shows such a time distribution, with the shaded area representing the range that would be used. The integral is divided by the product of the integration interval and the number of events over which the distribution was accumulated. Deviation from a perfectly flat distribution over this range would be indicative of a problem.

Benefits of the integral method

- Automatically includes the same TDC deadtime effects that necessarily exist in the yield. This is, perhpas, the most compelling reason for making the integral method the primary means of calculating the flux.

- Can be used for both high rate and low rate detectors.

Problems with the integral method

- Tends to throw away a lot of data. Particularly for high rate detectors.

- For abstract detectors (those formed via software coincidence), the LIFO and deadtime effects may enter in a subtle way that is difficult to detect or correct for.

6.4.3 The Poisson Method

It is known that the possibility of the number of random occurrences of some phenomenon like the nuclear decay in a specified unit of time should follow the poisson distribution. As is discribed in Section.6.4.1, the possibility of number of hits in the certain TDC time window Δt with given rate R should behave like the nuclear decay possibility is also distribute like the poisson. The idea is to estimate R from a number of hits distribution in the TDC gate. This is another way of estimate the ditector fireing rate.

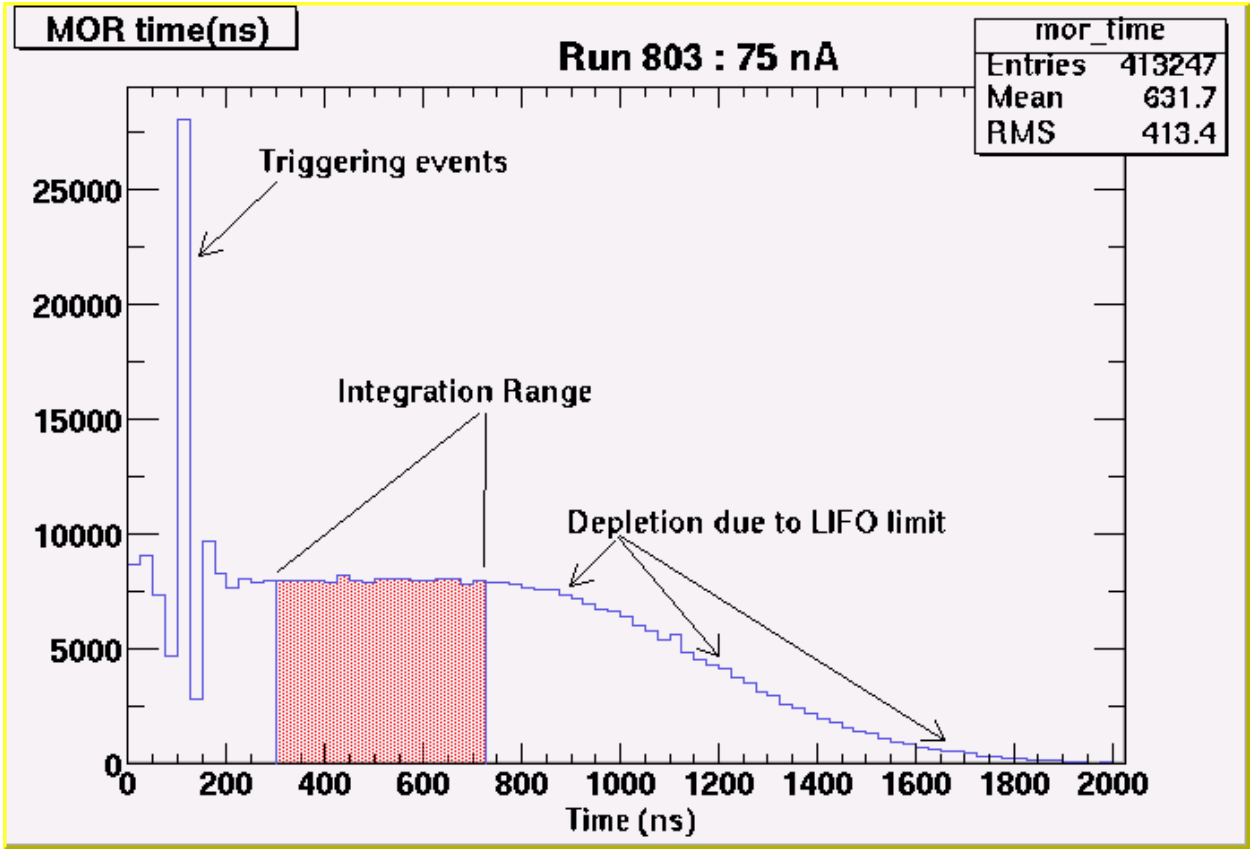

Figure 12: MOR (hardware OR of top 19 Tagger T-counters) time distribution. The shaded area represents the range of integration as described in section 6.4.2.

6.5 Errors

There are two sources for errors in counting the number of electrons in the tagger. The first is instability in the beam current which leads to a systematic overestimation of detector rates. This is described in section 6.5.1. The second is statistical in origin and is described in section 6.5.2.

6.5.1 Systematic Errors Due to Beam Instability

Beam Current Oscillation Use of a sampling technique can lead to overcounting if sampling times are correlated with the source intensity. More specifically, since the trigger rate is beam dependant, the number of samples taken per unit time will then also be beam dependant. Thus, if we have more samples at high rates than at low rates, the average rate we calculate will be higher than the true average.

This effect can be calculated for the case of a beam current which oscillates about an average value. Assume a beam current of the form $I_{beam} = I_o + \alpha sin\omega t$. The frequency ω is assumed to be large enough that many oscillations occur over the course of a run yet small enough that the rate is essentially constant over the sampling window (typically around 10 μs).

The PrimEx trigger is dominated by accidentals from Compton scattering in the target, the window of the vacuum box, and the helium inside of the helium bag. This means the trigger rate will be proportional to the beam current squared:

$$R_{trigger} \propto (I_{beam})^2$$

Assuming hits in the tagger are dominated by good electrons, the tagger rates will increase only linearly with the beam current:

$$R_{det} \propto I_{beam}$$

The number of hits a detector sees over the course of the run will then be:

$$N_{hits} = \int_0^T W_{OOT} R_{det} R_{trigger} dt = C \int_0^T (I_o + \alpha sin\omega t)^3 dt$$

where W_{OOT} is the out of time window width and T is the total astrological time of the run(ignoring the DAQ livetime for the purposes of this calculation). C is a proportionality constant which includes W_{OOT}. Integration yields:

$$N_{hits} = CT(I_o^3 + \tfrac{3}{2} I_o \alpha^2)$$

The first term gives the number of hits which would be recorded for the case when $\alpha = 0$. The fractional increase in the number of hits recorded is then given by:

$$\frac{N_{hits}^{measured} - N_{hits}^{actual}}{N_{hits}^{actual}} = \frac{3}{2}\left(\frac{\alpha}{I_o}\right)^2 \tag{8}$$

Take, for example, the case when α is 10% of I_o. The number of hits recorded will be increased by $3/2(0.010 I_o/I_o)^2 = 0.015$ or 1.5%.

Beam Current Drift Occasionally, a very slow drift can be observed in the beam current that becomes significant over time. Assuming a beam current of the form $I_{beam} = I_o - \beta t$, the above calculation can be repeated for an integration period of $-T/2$ to $T/2$. The resulting number of hits is:

$$N_{hits} = CT(T_o^3 + \tfrac{1}{4} I_o \beta^2 T^2)$$

The fractional increase in the number of hits due to beam drift is then given by:

$$\frac{N_{hits}^{measured} - N_{hits}^{actual}}{N_{hits}^{actual}} = \frac{1}{4}\Big(\frac{\beta T}{I_o}\Big)^2 \tag{9}$$

As an example, consider a period for which the beam drifted down by 20% before it was corrected. The number of recorded hits will be overcounted by $\frac{1}{4}(0.20 I_o/I_o)^2 = 0.01$ or 1%. This can be controlled somewhat during the analysis by reducing the time slices over which the counts are integrated. One might also try and detect such drifts and either remove the affected data, or correct for the effect.

6.5.2 Statitical Errors

Each of the three methods described in 6.4 has its own error bar associated with it. The errors on each of the methods can be propagated using the standard $1/\sqrt{N}$ for counted values and $\pm 0.5ns$ for time windows where appropriate.

More discussion on this is needed to determine the correct approach *The situation is the following: If we have 3 different methods to determine the same thing, do we use a weighted averag eof the three for the final number and error bar? Or, do we just choose the one with the smallest error bar and point to the others as confirmation (assuming the error bars overlap)? One complication to this is that in order to compare the integral method with the exponential, a software imposed deadtime must be imposed. Therefore, any weighted average would require the same software deadtime be imposed on events in the yield. This would throw away some valid Primakoff events. Possibly very few, depending upon the deadtime used.*

6.6 Summary

6.6.1 JLab beam current stability

7 Trigger selection for luminosity monitoring events (D. Sober, E. Pasyuk, D. Dale, D. Lawrence)

In addition to the tagger, there are three basic detector systems involved in luminosity monitoring events – HYCAL, total absorption counter, and the pair spectrometer. In advance of the run, it must be explicitly determined which triggers will be in the data stream, and what the relevent prescale factors should be.

7.1 Pair spectrometer rates with a MOR trigger

In considering the run times for the pair spectrometer triggered on the MOR, one must take into account that due to DAQ deadtime considerations, the DAQ data rate will be about 3000Hz. With a 5% X_o converter, the efficiency of the pair spectrometer to tag a 4-6 GeV photon is about 0.5%. This corresponds to a pair spectrometer rate of 15 Hz. For 20 T counter with 1% statistics, this corresponds to about four hours of running.

8 Target thickness measurements (R. Miskimen)

Three experimental targets will be employed in the PrimEx experiment – ^{12}C, ^{120}Sn, and ^{208}Pb – each 5% of a radiation length in thickness. In the Primakoff process the reaction mechanism is simplified if the target nucleus has $J^\pi = 0^+$. Therefore, isotopically enriched materials are required for the tin and lead targets. The ^{120}Sn and ^{208}Pb targets were ordered from Oak Ridge National Laboratory at a cost of approximately $12.5k and delivered in early summer of 2001. The enrichments are 98.29% for the tin target, and 99.09% for the lead target.

In this experiment, we require that the target thickness, ρ_t, be known to a precision better than $\pm 0.7\%$. In principle this tolerance can be satisfied by micrometer measurements with an accuracy of ± 0.05 mil, and micrometers of this accuracy are commercially available. However, use of a micrometer could produce indentations or bends in the metal foils. For this reason we plan to perform direct measurements of the metal foils with a technique that avoids direct contact with the target. X-ray attenuation represents the basis for such a determination. In this technique a line source of X-rays is collimated to a spot size a few mm in diameter and detected in a NaI detector behind the target foil. For these measurements we use the 60 keV X-ray line from ^{241}Am. The attenuated X-ray intensity through the foil is given by:

$$I(T) = I_0 B(T) e^{-T/\lambda}$$

where I_0 is the unattenuated intensity, T is the target thickness, λ is the X-ray attenuation length, and B(T) is the buildup factor. Provided that λ and the functional dependence of the buildup factor on T are known, T can be obtained from a measurement of the attenuated X-ray flux through the target foil.

Purely exponential attenuation, where the buildup factor B(T) is unity, is only realized in a situation where the X-ray collimation is perfect and the X-ray detector subtends zero solid angle. In more realistic situations, Compton scattering in the target foil leads to non-exponential attenuation. Using 60 keV X-rays and tin and lead foils of approximately 5% radiation lengths in thickness, we found that the buildup factor can be empirically parameterized by

$$B(T) = 1 + bT/\lambda$$

where b is a constant, approximately 0.07 for tin, and 0.15 for lead. Therefore, the flux decreases more slowly with increasing foil thickness than for pure exponential behavior. We

found no evidence that higher order terms in T/λ play a significant role in the buildup factor for 5% radiation length targets.

To calibrate the measurements, we plan to first make a micrometer measurement at one point on the target and then to X-ray that point. This provides a calibration for the parameter b. The X-ray attenuation lengths are known with sufficient accuracy at 60 keV for tin and lead, at about the 1% level, and can be taken from the literature. Then other points of the target are X-rayed and the target thickness obtained from the attenuated X-ray flux. We plan to take a micrometer measurement on at least one other point of the target to cross calibrate the procedure.

The targets will be scanned over the X-ray source to obtain a map of ρ_t as a function of x and y. Scanning a thick high-Z wire through the beam fiducializes the position of the X-ray beam. In this case we look for a dip in the count rate as the wire passes through the X-ray beam.

The X-ray scan apparatus has been designed and constructed and is controlled by LabView. A 1" NaI crystal is used to the detect X-rays and the NaI pulse height is readout through a CAMAC ADC system, also running under LabView control. We plan to complete thickness measurements of the tin and lead targets in the Summer of 2002.

The carbon target will be machined from a block of pyrolytic graphite (PG) of natural isotopic purity. PG is a crystalline form of graphite that is produced using high temperature Chemical Vapor Deposition furnace technology. The low porosity of PG, approximately 1%, as compared to 10% for normal graphite makes it an ideal material for use as a target. The PG density depends somewhat on the specifics of the manufacturing process. However, PG densities are typically close to the theoretical limit of 2.25 g/cm^3. We plan to measure the density of the PG target in a specific gravity setup using an electronic scale and ultrapure water. Laboratory tests have indicated that we can achieve the required level of precision for the density. The thickness of the target (approximately 1 cm) will be measured with a micrometer; a prototype target machined from a block of normal graphite had thickness variations of approximately 0.1%. Finally, as a last check on ρ_t, we plan to X-ray the carbon target to make sure there are no internal voids in the PG material.

We have obtained a sample of PG from SLAC that is sufficiently large that several targets can be cut from it. A target has been successfully machined from the sample.

The PrimEx target ladder and moving mechanism have been designed, constructed and assembled by the JLab technical staff. The target ladder can move in both the horizontal and vertical directions, giving us fine control over exactly where we place the photon spot on the target. There are positions on the target ladder for six targets – the three production targets, a blank, a crossed wire to fiducialize the position of the photon beam by use of pair production, and a thin foil to be used in tests of the pair spectrometer.

9 Normalizing Primakoff yield to Compton yield (D. Dale)

9.1 The basic idea

Here, we argue that an alternative technique for determining the absolute Primakoff cross section can be employed which is largely insensitive to the degree in which we can determine the absolute target thickness and absolute tagged photon flux. This involves measuring the Primakoff π^o yield relative to the Compton yield. This could greatly reduce the major sources of error in the experiment – photon flux, (1% error) and target thickness, (0.7% error).

The Primakoff cross section is given by:

$$\frac{d^3\sigma_P}{d\Omega} = \Gamma_{\gamma\gamma}\frac{8\alpha Z^2}{m^3}\frac{\beta^3 E^4}{Q^4}|F_{e.m.}(Q)|^2 \sin^2\theta_\pi, \tag{10}$$

and the experimental Primakoff yield can then be expressed as:

$$Y_{\pi^o} = t_{target} \times \Phi_\gamma \times \Gamma_{\gamma\gamma} \times Z^2 \times \sigma_p, \tag{11}$$

where σ_p represents known constants and kinematical factors which are integrated over the (two photon) acceptance of the HYCAL detector, t_{target} is the target thickness, and Φ_γ is the tagged photon flux.

This Primakoff yield can be measured with respect to the yield of Compton scattered photons (off of atomic electrons in the target). The idea behind using electron Compton scattering comes from the fact that it is a calculable, pure QED process. The cross section is given by the Klein-Nishina formula:

$$\frac{d\sigma}{d\Omega} = Zr_o^2\frac{1+cos^2\theta}{2}\frac{1}{1+\gamma(1-cos\theta)^2}[1+\frac{\gamma^2(1-cos\theta)^2}{(1+cos^2\theta)(1+\gamma(1-cos\theta))}] \tag{12}$$

Or, one could write:

$$Y_{Compton} = t_{target} \times \Phi_\gamma \times Z \times \sigma_{Compton}, \tag{13}$$

Taking the obvious ratio, we get:

$$\frac{Y_{\pi^o}}{Y_{Compton}} = Z \times \Gamma_{\gamma\gamma} \times \frac{\sigma_P}{\sigma_{Compton}}, \tag{14}$$

independent of the target thickness and tagged photon flux.

9.2 Identification of the Primakoff events

For such a technique to work, we must be able to cleanly (to better than the 1% level) identify the Compton events in the HYCAL. The most "Compton-like" background is pair production followed by bremsstrahlung. Any technique used must provide a clean separation

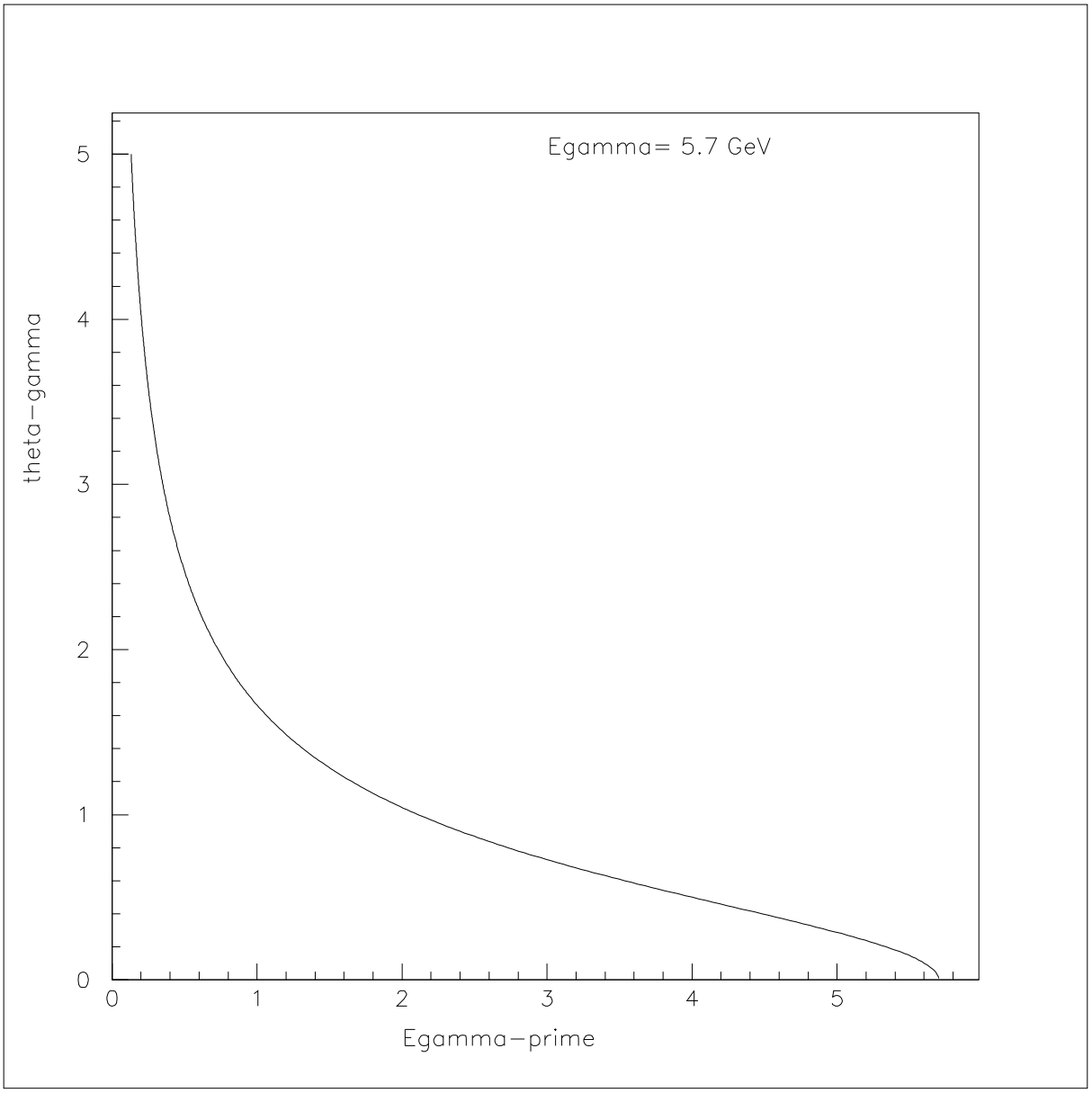

Figure 13: Kinematical correlation between Compton scattered photon energy and scattering angle.

between Compton scattering and such backgrounds. In the simulations discussed here, I will make use of the kinematical correlation between the scattered photon and its energy shown in figure 13.

I have taken the following detector resolutions for the HYCAL:

$PbWO_4$:

$$\frac{\sigma(E)}{E} = \frac{3\%}{\sqrt{(E)}} \tag{15}$$

$$\sigma(r) = \frac{2.5mm}{\sqrt{(E)}} \tag{16}$$

and

Lead Glass:

$$\frac{\sigma(E)}{E} = \frac{6\%}{\sqrt{(E)}} \tag{17}$$

$$\sigma(r) = \frac{5mm}{\sqrt{(E)}} \tag{18}$$

where E is the energy in GeV. All simulations shown here are for a 5% radiation length carbon target. The HYCAL was $1m \times 1m$ and the central hole in the detector was $8cm \times 8cm$.

First, I looked at the case where all physics processes in the target are turned off except Compton scattering. I triggered 10 million $5.7GeV$ photons on target which resulted in 305 Compton events with energy above $1GeV$ (the approximate threshold for the data taking) registering in the HYCAL. This gives on the order of $500Hz$ of Compton events across the tagger focal plane in our experimental conditions. The resulting distribution of events in scattered photon energy and angle is shown in figure 14. A cut was imposed in $E_{\gamma'} - \theta_{\gamma'}$ space to identify the Compton events. This is shown in figure 15.

Figure 16 shows the situation with all physics processes (and thus all backgrounds) turned on. The same number (10 million) of photons were incident on the target as in figures 14 and 15. In this case 255 events passed the Compton cuts with a 1 GeV threshold (as opposed to 305 with just Compton turned on) and 22 lay outside the Compton cuts. It is worth considering two competing effects here. The first is the contamination of the region defined by the Compton cuts with non-Compton related events. The second is the loss of registered Compton events due to two step processes such as Compton scattering followed by pair production of the outgoing Compton scattered photon. For a 5% radiation length target, the latter effect should be about 3%, and can be adequately corrected for with even a crude knowledge of the target thickness.

The number of non-Compton related events which fall within the Compton cuts was studied by leaving on all physical processes in the GEANT simulation except Compton scattering. This is shown in figure 17 where 10 million photons on target are triggered. The GEANT simulation has an energy threshold of $0.1GeV$. For an energy cut of $1GeV$ such as we will have in the data taking, 2 events pass the Compton cuts corresponding to about $3Hz$

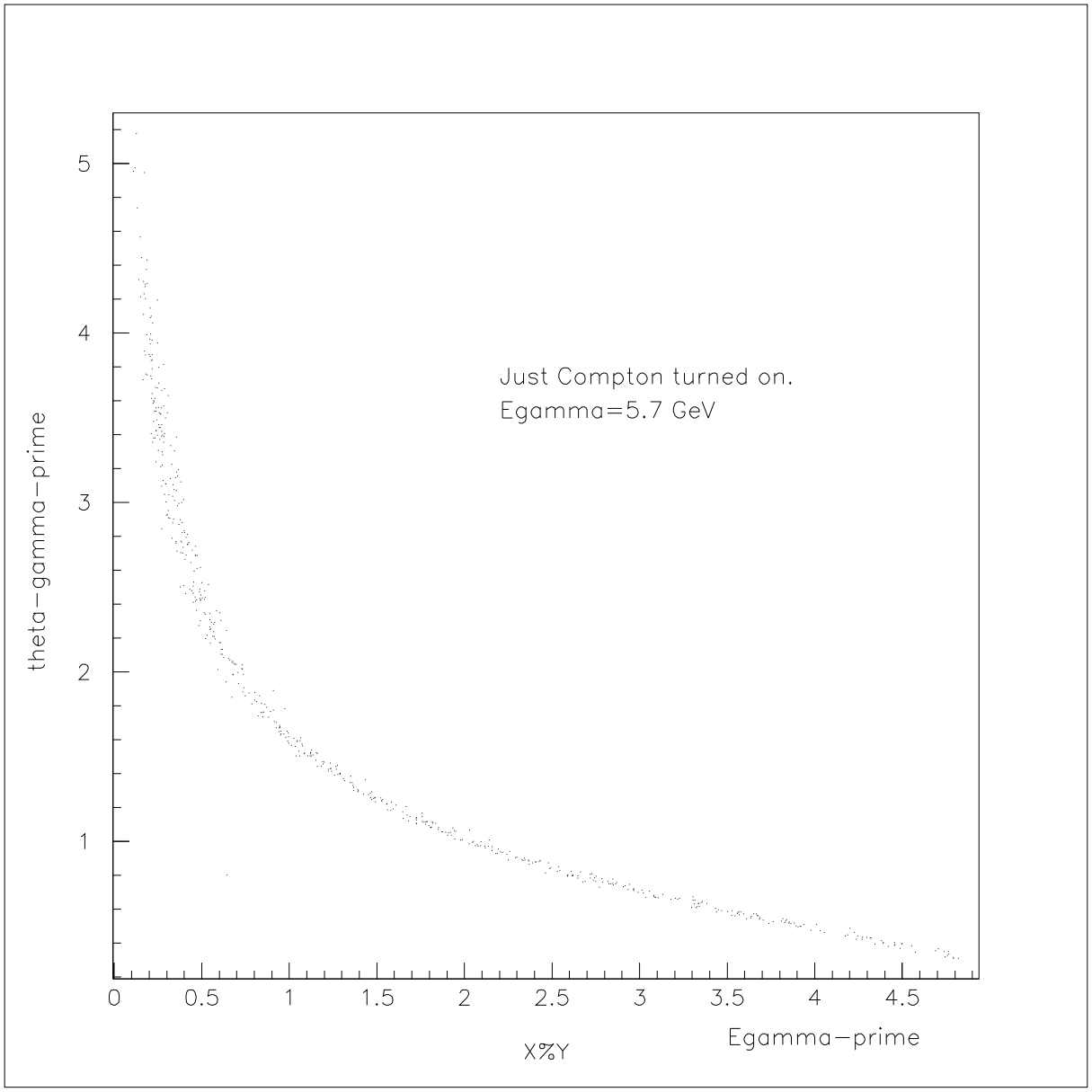

Figure 14: Kinematical correlation between Compton scattered photon energy and scattering angle as generated by GEANT. Only Compton scattering is turned on in the simulation.

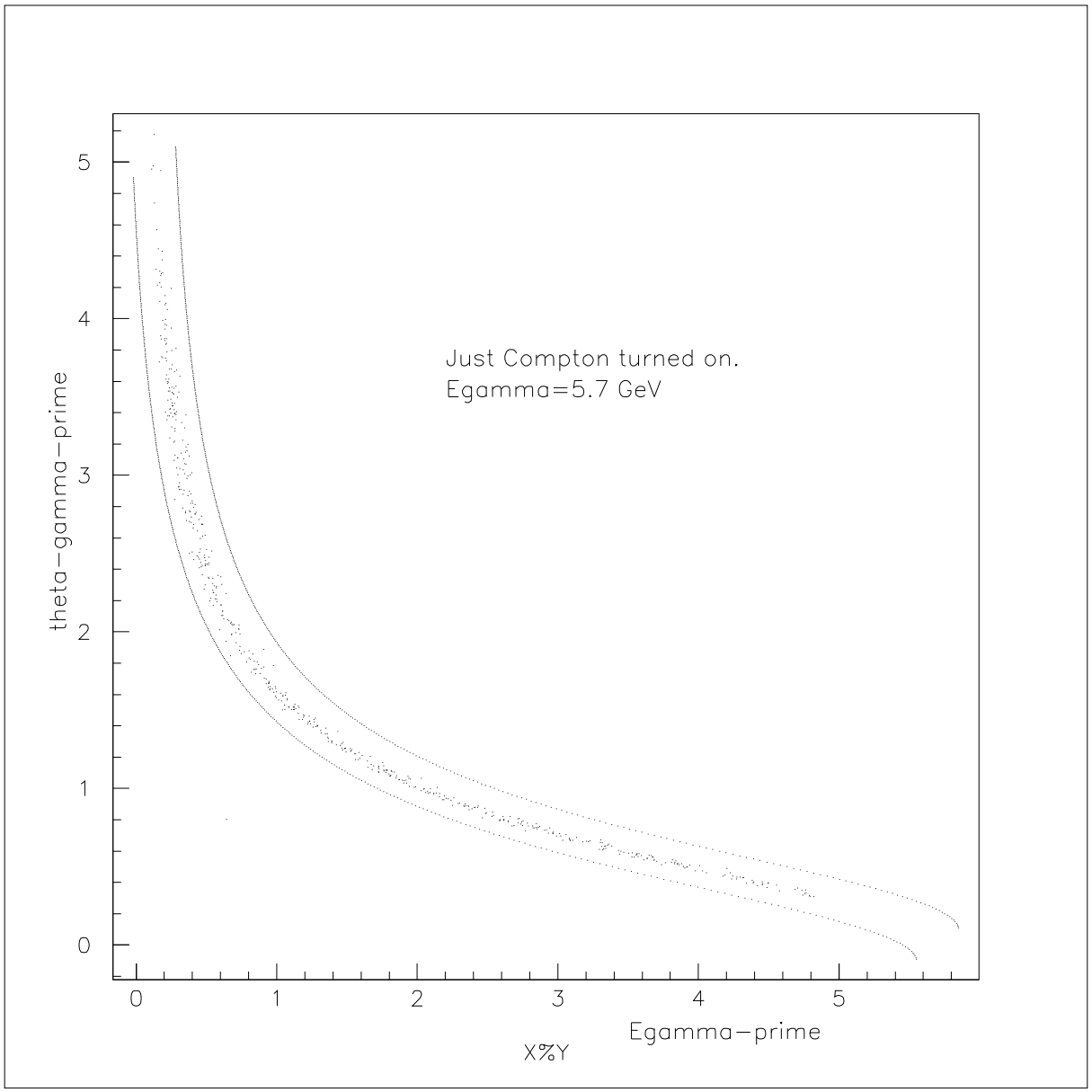

Figure 15: Cuts used in $E_{\gamma'} - \theta_{\gamma'}$ space to identify the Compton events.

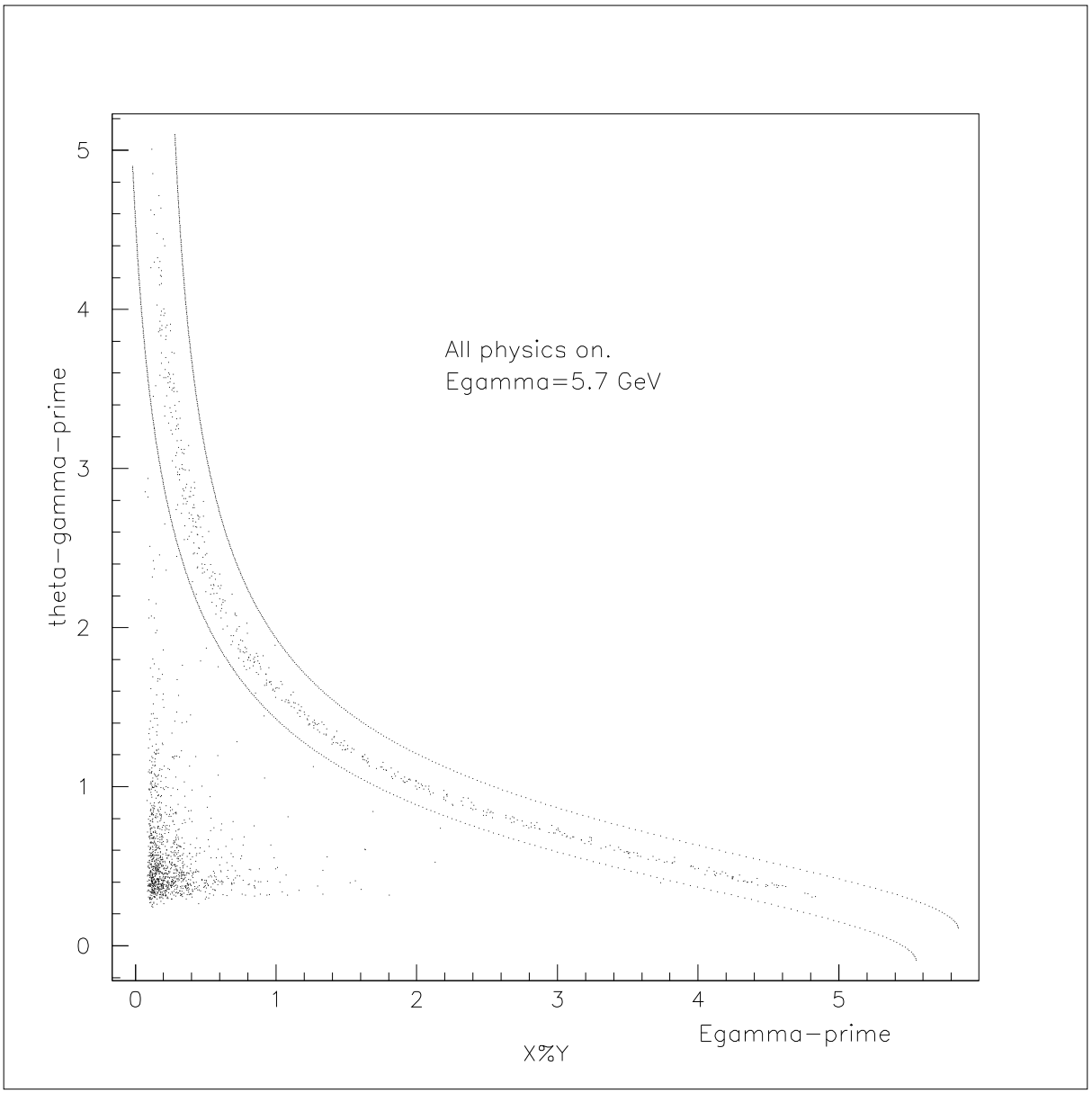

Figure 16: Kinematical correlation between Compton scattered photon energy and scattering angle as generated by GEANT. All physics processes are turned on, and the "Compton event" cuts are shown.

of events improperly identified as Compton events. With a Compton rate of about $500Hz$, this implies a less than 1% background to the Compton process.

Photon singles rates due to hadronic production will also be an issue. In the PrimEx proposal presented at PAC15, total singles rates from ω production were estimated to be less than 1 Hz (figure 26c of the proposal), with those from ρ production estimated to be about ten times those of the ω. This compares favorably with the 500 Hz Compton rate.

9.3 Sensitivity of method to energy calibration

This method relies on measuring the ratio of Primakoff production to Compton scattering. Since the cross section for Primakoff production increases with energy, and the cross section for Compton scattering decreases with energy in this energy range, the ratio will be more sensitive to the energy calibration than Primakoff production alone. This is shown in figure 18. The plot indicates that a 1% error in incident photon energy gives a 1% error in the π^o radiative width. Thus, the effectiveness of this technique is directly tied to the energy calibration. To compare this to the sensitivity of the Primakoff yield to photon energy, figure 19 shows the Primakoff yield (again integrated out to 2 degrees) as a function of photon energy. Here, it can be seen that a 1% error in photon energy calibration gives a 0.3% error in the Primakoff yield.

9.4 Sensitivity to HYCAL central hole size

The acceptance of Compton events is considerably more sensitive to the size of the central hole in the fiducial volume of HYCAL than the Primakoff acceptance. Figure 20 shows the relative Compton acceptance *versus* the central hole size, where it can be seen that a $1mm$ error gives a 0.5% error in the Compton yield. While there is some cancellation of this error in taking the Compton to Primakoff ratio, this cancellation is, quite small, as is shown in figure 21. Thus to use this technique, one must know the detector fiducial volume as precisely as possible.

9.5 Conclusion

This technique shows promise as an alternative to that relying on the TAC and the pair spectrometer. It requires no new major instrumentation or beam time. It's main advantage is that it essentially eliminates the need to know the target thickness and tagged photon flux. The two main drawbacks are:

- Increased sensitivity to photon energy calibration.
- Sensitivity to knowledge of fiducial volume of HYCAL.

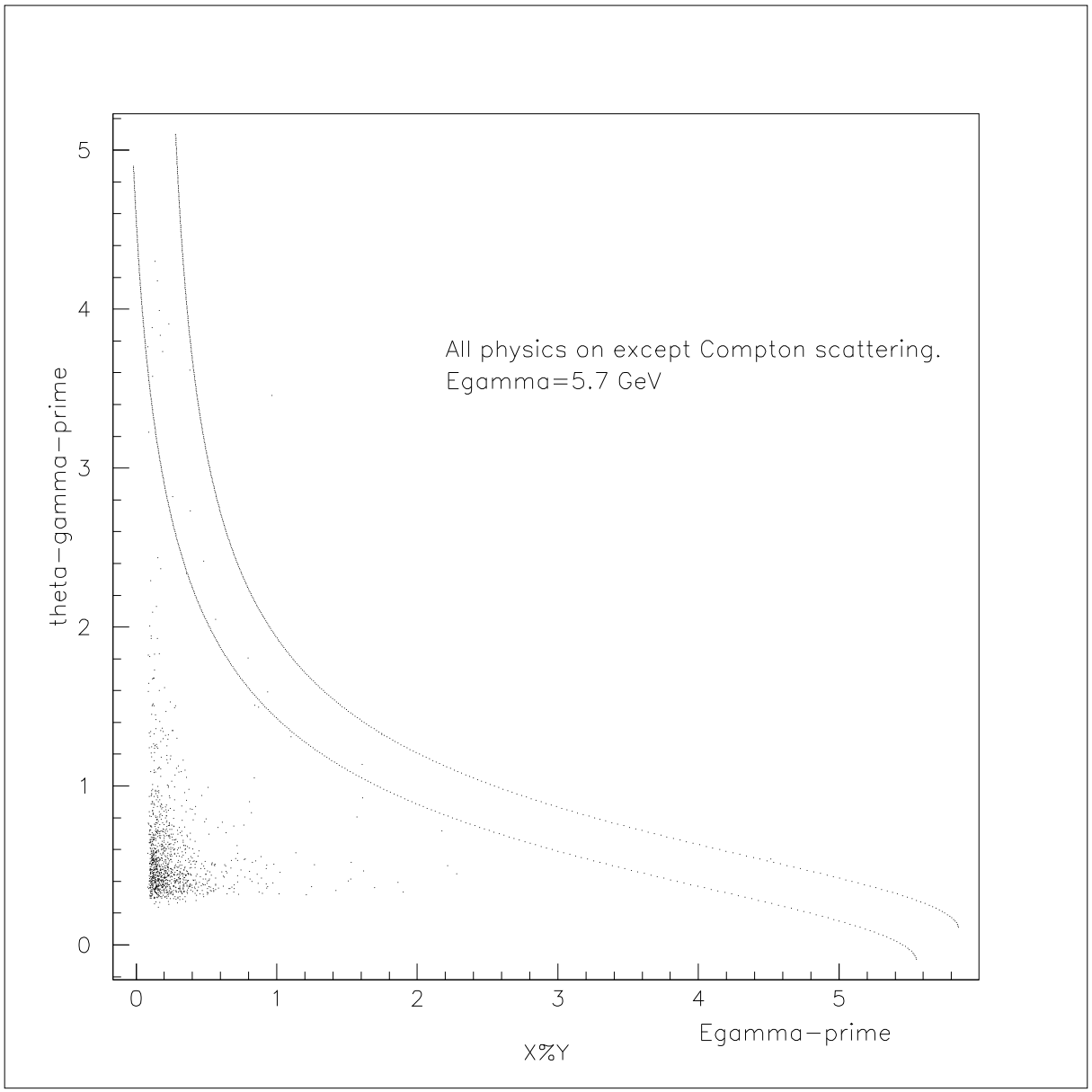

Figure 17: Kinematical correlation between photon energy and angle as generated by GEANT. All physics processes are turned on *except* Compton scattering, and the "Compton event" cuts are shown.

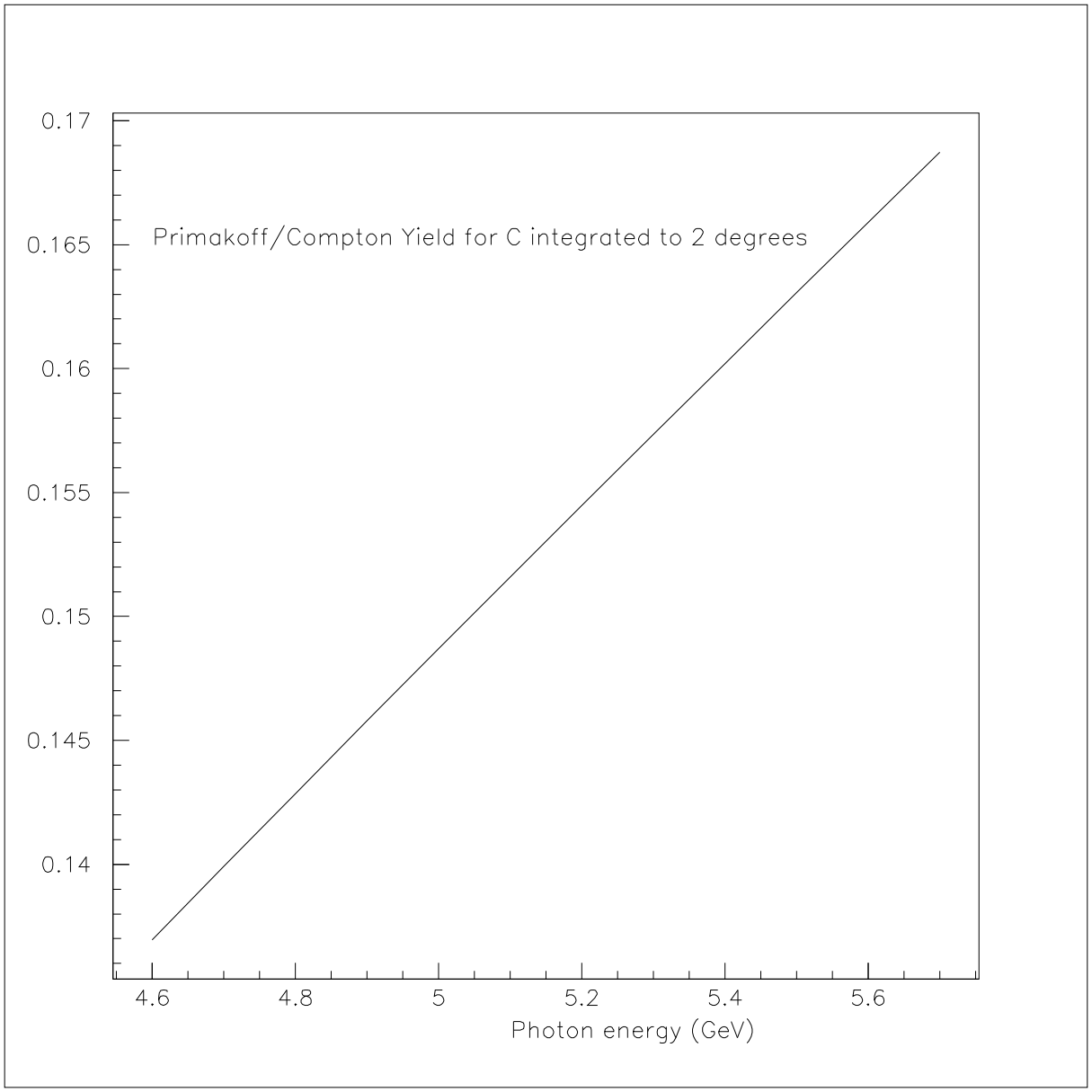

Figure 18: Ratio of Primakoff yield to Compton yield, each integrated out to 2.0 degrees.

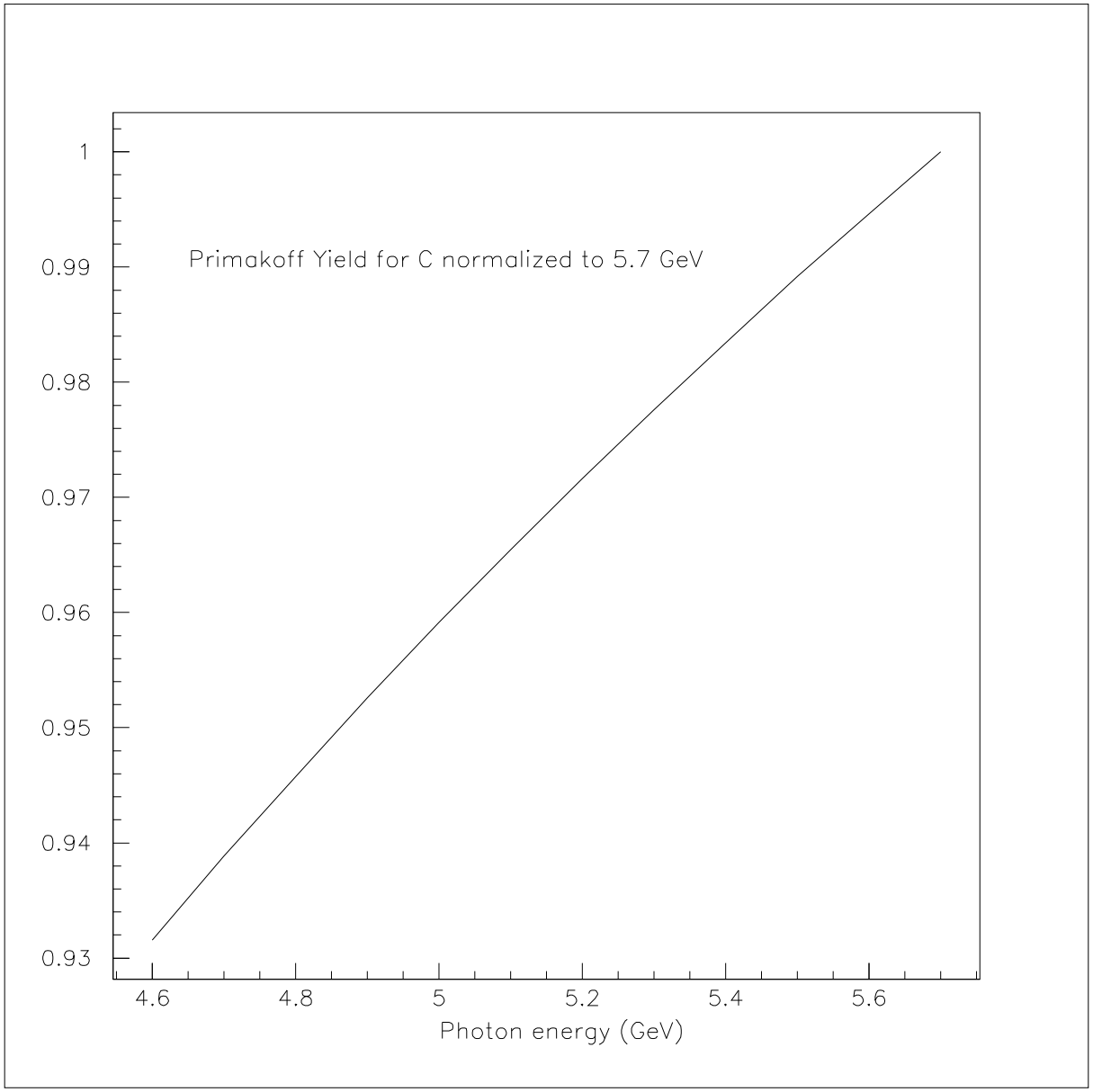

Figure 19: The Primakoff yield (normalized to 5.7 GeV) *versus* incident photon energy.

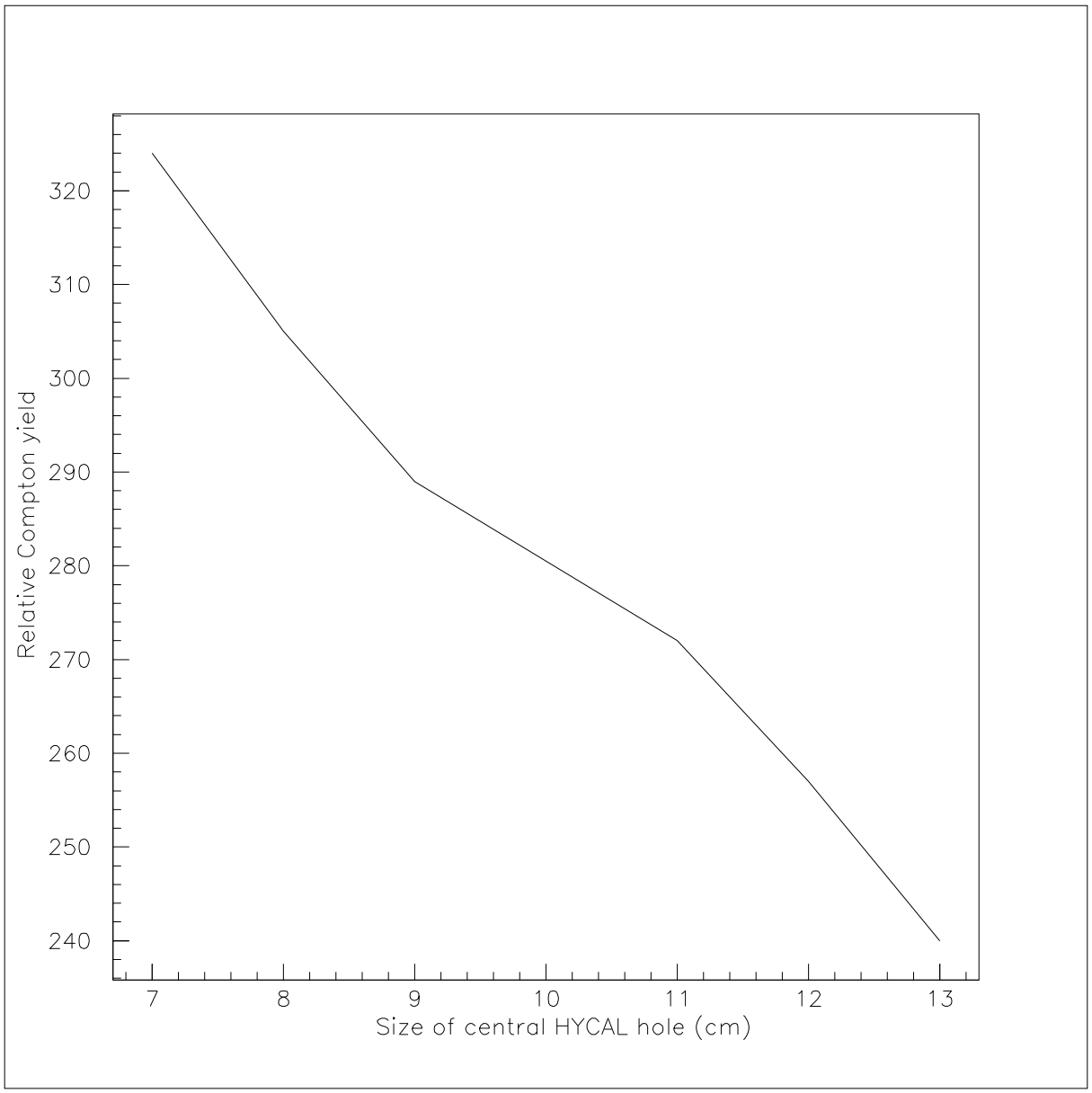

Figure 20: The relative Compton yield above 1 GeV scattered photon energy *versus* the size of the central hole in the fiducial volume of HYCAL.

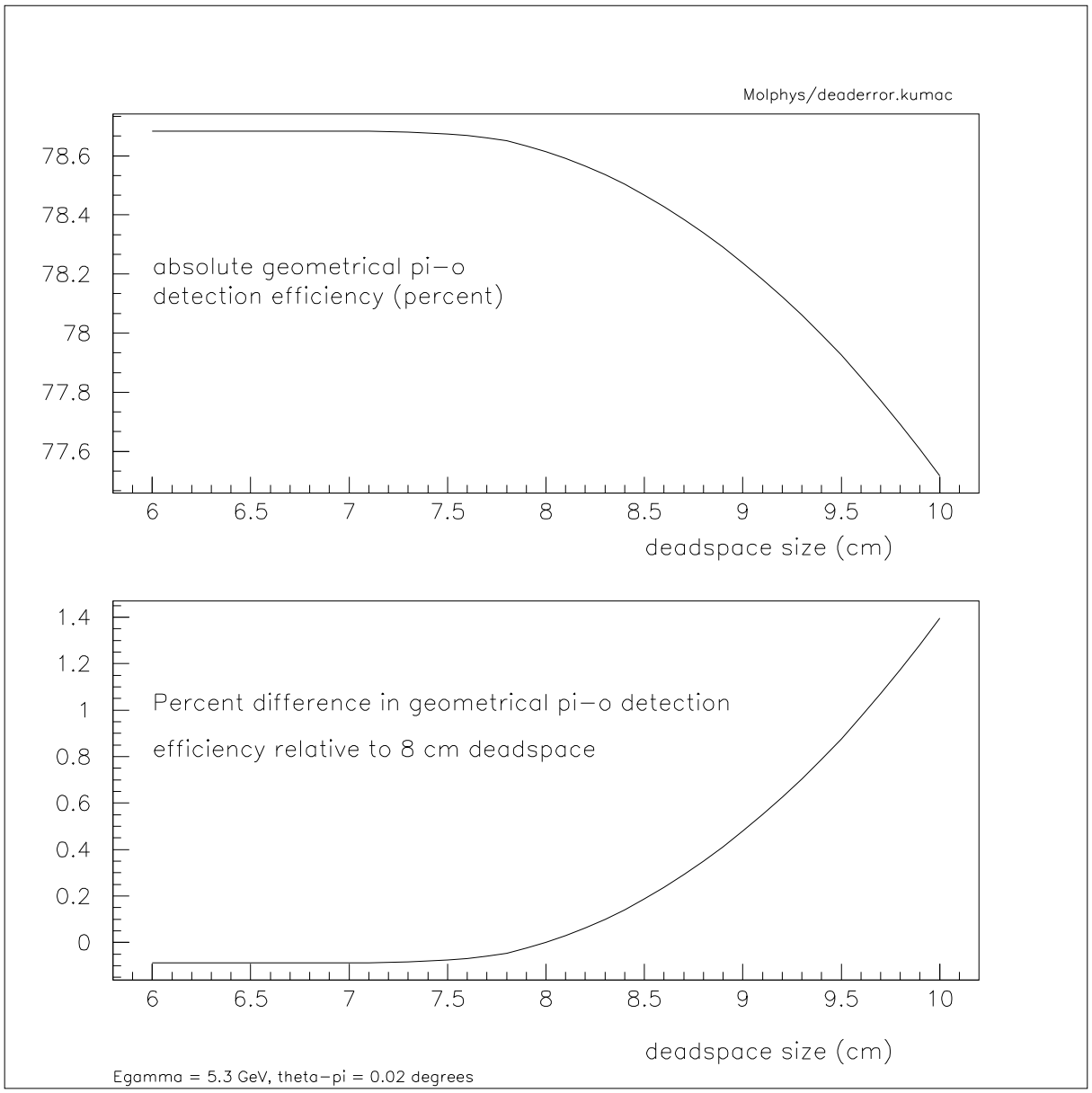

Figure 21: The relative Primakoff yield *versus* the size of the central hole in the fiducial volume of HYCAL.

10 Beamline instrumentation

The exact configuration of the various beamline monitors must be determined. This is the information I (DSD) have available at present.

10.1 Electron beam position monitors

There are two cavity electron beam position monitors upstream of the tagger. They are 50 feet apart and have an accuracy of $\pm 50\mu m$. Their stability depends on the beam current. At 1-2 nA, they are stable to within $\pm 50\mu m$.

10.2 Harp

The following information about the photon harp I (DSD) don't yet understand.

Photon Harp: the wire (tungstane) width: 100 um
wire thickness: 200 um (a band)
number of steps accross the beam: 10
statistical accuracy of the beam centroid and width: ¡10 um
pair spectrometer counters are in use for detection
min beam current: 50 pA. Alwais one can make a wire thicker

10.3 Online scintillating fiber based profile monitor (Liping)

Downstream of the HYCAL, there will be a scintillating fiber online photon beam position and profile monitor.It will consist of two arrays of 2 mm fibers oriented at 90 degrees to one another for $x - y$ position determination. Each array will have 64 fibers which will be read out from internal amplifier-discriminators. The signals will be sent to scalers which will be read in EPICS at 1 to 2 Hz, providing online monitoring of the centroid and width of the beam. This informstion will also be in the data stream. Each fiber can be read out at up to 10 MHz.

11 Future test run plans

There is a variety of things that we need to do before getting production beam time. They are:

- TAC runs with largest possible range of currents.
  Understand absolute tagging efficiencies.
  Compare with simulations.
- TAC runs with different thresholds.

- Repeat what we have done with new E counter electronics.
- Determine N_{e_i} for TAC and pair spectrometer in manner we plan for experiment.
- Runs with different pair production target thicknesses.
- Implement ADC's for pair spectrometer detectors to study rate dependence of pulse heights.
- Commission more pair spectrometer detectors
- Runs with intentional 30 Hz beam intensity fluctuations. .
- Map relative target thicknesses over x and y with pair spectrometer.
- Measure Compton cross section:

  $\rightarrow$ Absolute luminosity.

  $\rightarrow$ Measure of relative target thicknesses of different Z targets.

12 Appendix I: Current Luminosity Monitoring Run-plan

13 Appendix II: Technical Details of Pair Spectrometer

13.0.1 Detectors

The full complement of pair spectrometer detectors required for the PrimEx run (16 telescopes or a total of 32 detectors) is constructed and installed in the Hall. For general use to the Hall B photon physics program, we are presently constructing an additional 16 telescopes to extend the range of photon energies which may be tagged.

Figure 22 shows a side view of a detector module. The front scintillators are $2.4cm \times 7.5cm$ and $0.5cm$ thick, and the rear scintillators are $9.3cm \times 3.1cm$ and $2cm$ thick. The photomultiplier tubes (front detectors: Hamamatsu R6427, rear detectors: R580-17) are shielded from magnetic fields with μ metal, and their voltage dividers have been modified to

enable extra power supplies to be applied to the last three dynodes for enhanced high rate capability.

A drawing of the detector assembly is shown in figure 23. The detector mounting system has been designed so as not to interfere with the geometrical acceptance of the HYCAL which is downstream of it, and the amount of material in the median plane of the magnet has been minimized using carbon composite material. A photograph of the detectors and support frame in the Hall is shown in figure 24.

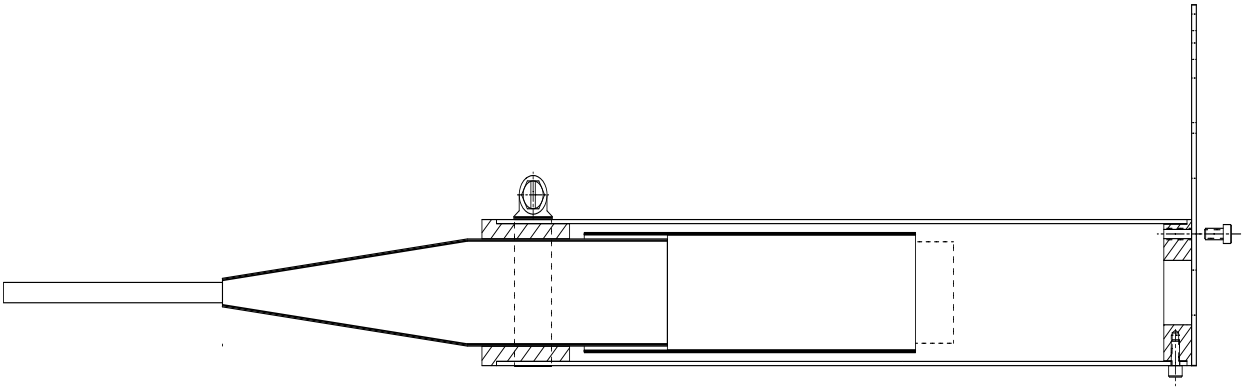

Figure 22: Side view of a front detector module. Scintillator (left, viewed edge-on), light guide (center), and photomultiplier tube (right) are all glued with optical cement. Patch panel for routing cables extends upward on the right.

The pair spectrometer and its associated data acquisition electronics has been installed, and is currently being commissioned. Preliminary commissioning was done during the $g8$ run in the summer of 2001, and partial commissioning was done in mid-September of 2001. A typical online plateau curve for a detector module, taken with beam, showing singles rates *versus* high voltage is shown in figure 25.

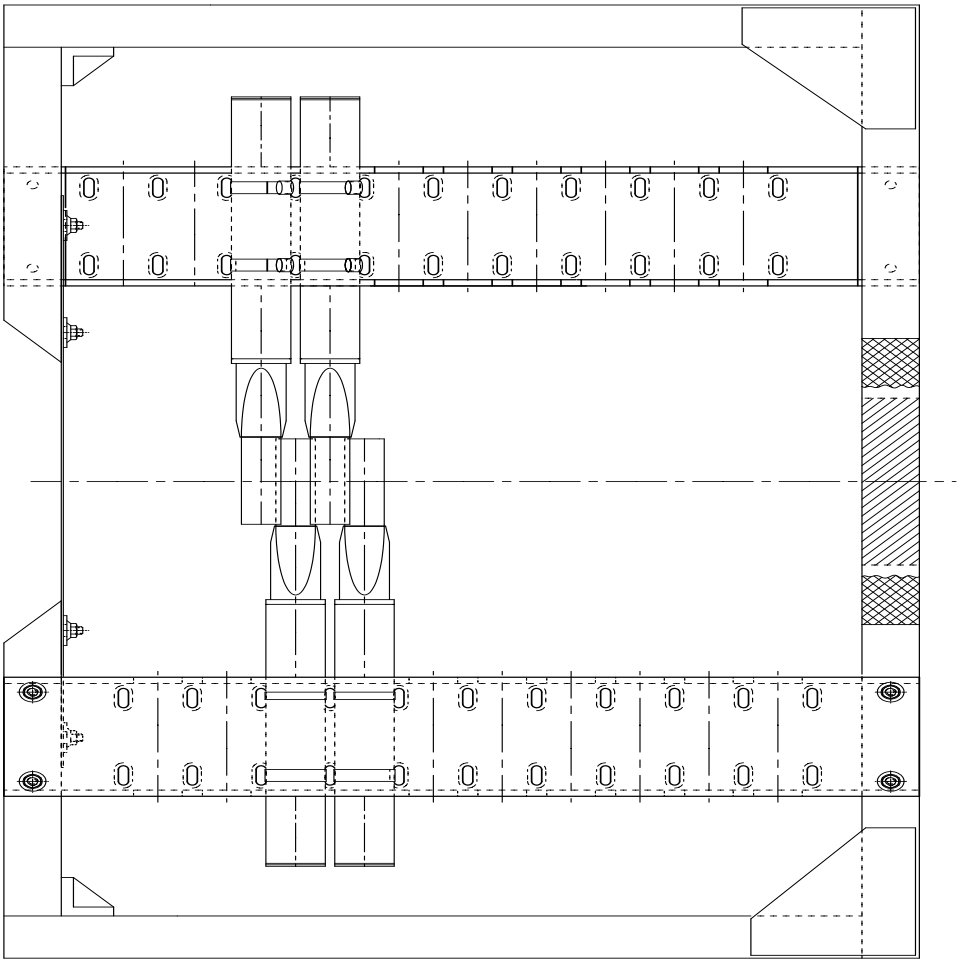

Figure 23: The pair spectrometer detector support frame, with four detectors shown mounted.

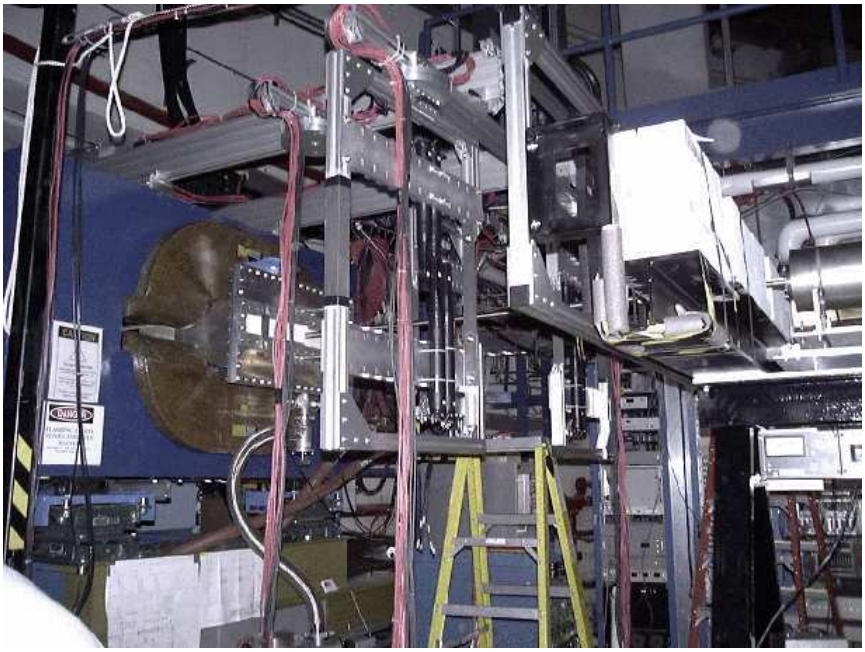

Figure 24: Pair spectrometer detectors and support frame being installed. The downstream side of the PrimEx/Hall B pair spectrometer magnet is on the left.

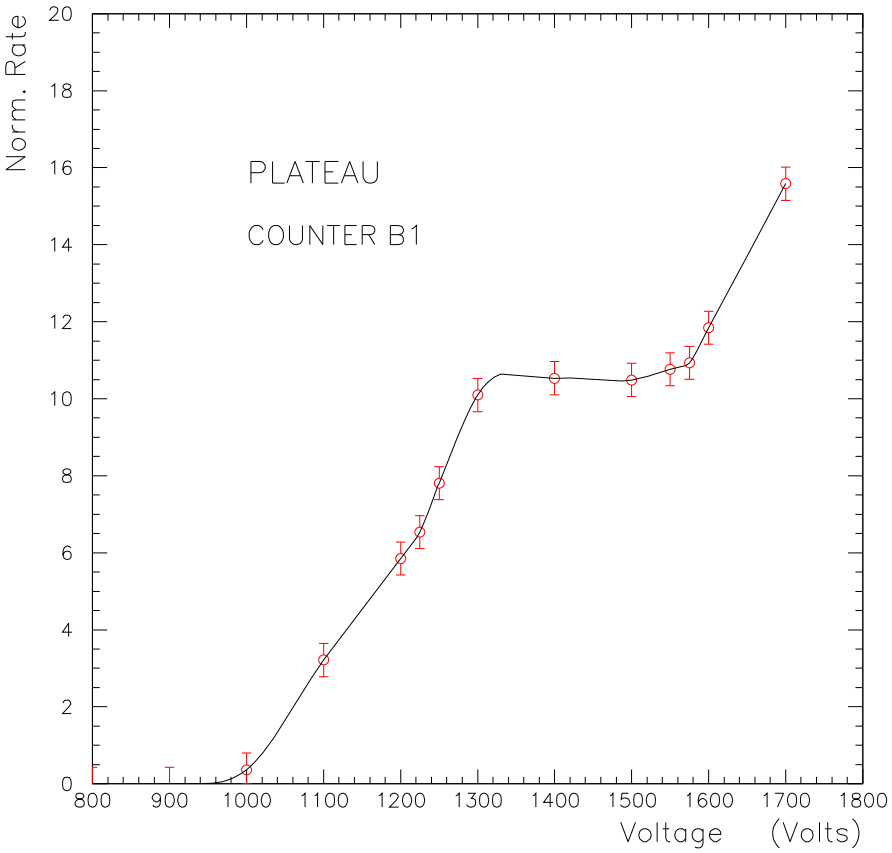

Figure 25: Typical online high voltage plateau curve for a pair spectrometer detector.